Design, detailing, and analysis of short-grouted ductile reinforcing bar connections for special precast concrete shear walls, part 1

Baha'a Al-Khateeb, Jon Mohle, and Yahya C. Kurama

- Design, detailing, and analysis recommendations are given for nonproprietary short-grouted ductile energy-dissipation bar connections in special seismic precast concrete shear walls, validated through experimental testing per the American Concrete Institute's (ACI's) *Requirements for Design of a Special Unbonded Post-Tensioned Precast Shear Wall Satisfying ACI 550.6 and Commentary*.
- A strut-and-tie model to design the connection tie reinforcement and grouted bar length is developed and validated, and simplified design equations are presented for practical engineering use.
- Results from fiber-element nonlinear numerical analyses as well as conventional closed-form sectional strength analysis methods are compared with experimental measurements to demonstrate that the behavior of precast concrete shear walls with short-grouted connections can be analyzed using standard reinforced-concrete modeling techniques.

This paper provides design, detailing, and analysis guidelines along with design examples (included as an accompanying article) for short-grouted ductile reinforcing bar connections across horizontal joints of special precast concrete shear walls. A previous study (Smith et al.[1]) highlighted the need for developing ductile grouted mechanical connections for yielding reinforcing bars (referred to as energy-dissipation bars) crossing the horizontal joints of special precast concrete shear wall structures. In accordance with this need, Aragon et al.[2–4] investigated nonproprietary short-grouted ductile reinforcing bar connections using straight and tapered steel ducts with and without corrugations. Results from a series of 20 single-bar connection specimens tested under uniaxial cyclic loading showed that adequate strength and ductility of the connection can be achieved using straight corrugated ducts with a connection bond length of nine times the bar diameter $9d_{ED}$ for no. 7 and 9 (22M and 29M) bars, and $12d_{ED}$ for no. 11 (36M) bars.

To investigate group and edge effects for the connections under in-plane reversed-cyclic lateral loading combined with superimposed axial loading, six shear wall specimens with multiple energy-dissipation bars crossing the base joint were subsequently tested by Al-Khateeb et al.[5,6] The performance of each specimen was evaluated in accordance with the applicable requirements of ACI 550.6-19, *Acceptance Criteria for Special Unbonded Post-Tensioned Precast Structural Walls Based on Validation Testing and Commentary*.[7]

Shear wall specimens 1 and 2 described in Al-Khateeb

et al.[5] did not meet the ACI 550.6-19[7] validation requirements because these walls failed to sustain three cycles at the validation-level drift without exceeding a 20% drop in lateral strength from the peak strength in each direction of loading. Design and detailing modifications implemented in specimen 3 improved the effectiveness of the tie reinforcement in the connection, leading to satisfactory performance and compliance of the wall with applicable ACI 550.6-19[7] requirements. The performance of specimen 3 demonstrated that the proposed connection can achieve ductile behavior of special precast concrete shear walls in high-seismic regions.

The second set of specimens described in Al-Khateeb et al.[6] (specimens 4, 5, and 6) evaluated the performance of the connection under varying parameters, including the energy-dissipation bar size, wall base moment-to-shear ratio M_b/V_b, wall thickness, axial load ratio, and layout of the energy-dissipation bars and tie reinforcement in the wall cross section. All of these specimens met the applicable validation requirements of ACI 550.6-19,[7] maintaining a relatively low damage condition at the end of the test despite undergoing large lateral displacements. Specimen 5 achieved ductile low-cycle fatigue fracture of an energy-dissipation bar, highlighting the high performance of the connections for seismic applications.

The experimental program was designed to rigorously test short-grouted ductile reinforcing bar connections under the most demanding in-plane loading that would be experienced in special shear walls with significant flexural yielding and cyclic compression/tension damage to the concrete. The specimen deformations also included significant shear sliding along the horizontal joint with the grouted connections, but the ultimate failure of the walls was not governed by shear friction. The authors believe that shear friction (sliding) failure of a wall would result in less demanding loading conditions on the grouted connections. Thus, it is deemed that the proposed connection can be used generally to connect precast concrete components both for shear friction and flexural yielding.

The nonproprietary short-grouted corrugated steel straight duct connection validated by this research uses vertical, transverse, and longitudinal tie reinforcing bars in the connection region. Unlike available proprietary grouted mechanical splices that use end-threaded reinforcing bars for force transfer along the splice, the energy-dissipation bars terminate inside the corrugated steel connection ducts, and the bar forces are transferred into the precast concrete component through the design and detailing of the surrounding tie reinforcement. A strut-and-tie model was originally developed by Aragon et al.[2–4] to design the tie reinforcement; this model was subsequently revised based on the testing of shear wall specimens 1 through 6 by Al-Khateeb et al.[5,6] and in accordance with the American Concrete Institute's (ACI's) *Building Code Requirements for Structural Concrete (ACI 318-19) and Commentary (ACI 318R-19)*[8] section 23.2.7.

The following sections of this paper summarize the strut-and-tie model in a form suitable for design practice, present recommended connection details, and provide closed-form section analysis methods for estimating the nominal and probable axial-flexural strengths of precast concrete shear walls using the proposed connection. Results from fiber-element nonlinear analyses of specimens 1 through 6 are compared with the experimental measurements to demonstrate that precast concrete walls with short-grouted energy-dissipation bar connections can be simulated numerically using conventional modeling methods. These design, detailing, and analysis recommendations represent an accumulation of the research findings from all of the single-bar connection tests[2–4] and the shear wall tests[5,6] conducted to date. In addition, design examples are presented in an accompanying paper[9] to demonstrate and clarify the connection design procedure. Ultimately, this paper provides engineers with the information needed to implement the proposed connection at base panel-to-foundation and upper panel-to-panel joints of high-seismic shear wall applications in practice. The cost-effectiveness and simplicity of this connection also make it viable for nonseismic applications, following the same design, detailing, and analysis recommendations presented herein. At upper panel-to-panel joints or in other applications where the connected flexural bars are designed not to yield, the required grouted connection length and connection tie reinforcement areas could potentially be reduced based on the development of the yield strength (rather than the ultimate strength) of the connected bars. However, these elastic reinforcing bar connections were not tested in this research program.

Connection design

The design of short-grouted connections for the energy-dissipation bars (that is, yielding flexural reinforcement) of a special precast concrete shear wall involves determining the connection length of the bars and the amount and placement of the vertical, transverse, and longitudinal tie reinforcement around the connections. The strut-and-tie model (**Fig. 1**) described in Al-Khateeb et al.[6] successfully achieved the design objectives for the strength and ductility of the grouted connections per the applicable performance requirements of ACI 550.6-19.[7] The equations from that strut-and-tie model can be used to derive simplified design equations for practice as described in this paper. The connection tie reinforcement is designed separately from the concrete confinement reinforcement (hoops and ties) in special boundary elements but should be detailed to integrate with the boundary reinforcement designed according to ACI 318-19[8] section 18.10.6.4.

Figure 1 and other associated figures in this paper depict placement of the connections inside a wall panel. This is a more critical condition than the placement of the connections inside the foundation (for the base connection of a shear wall) because the relatively large foundation allows more space and better confinement for the connection ducts and tie reinforcement. Placement of the connections inside the foundation would be preferred for the base joint of a wall. In this case, the design equations remain the same, but the connections are oriented so that the energy-dissipation bars extend from

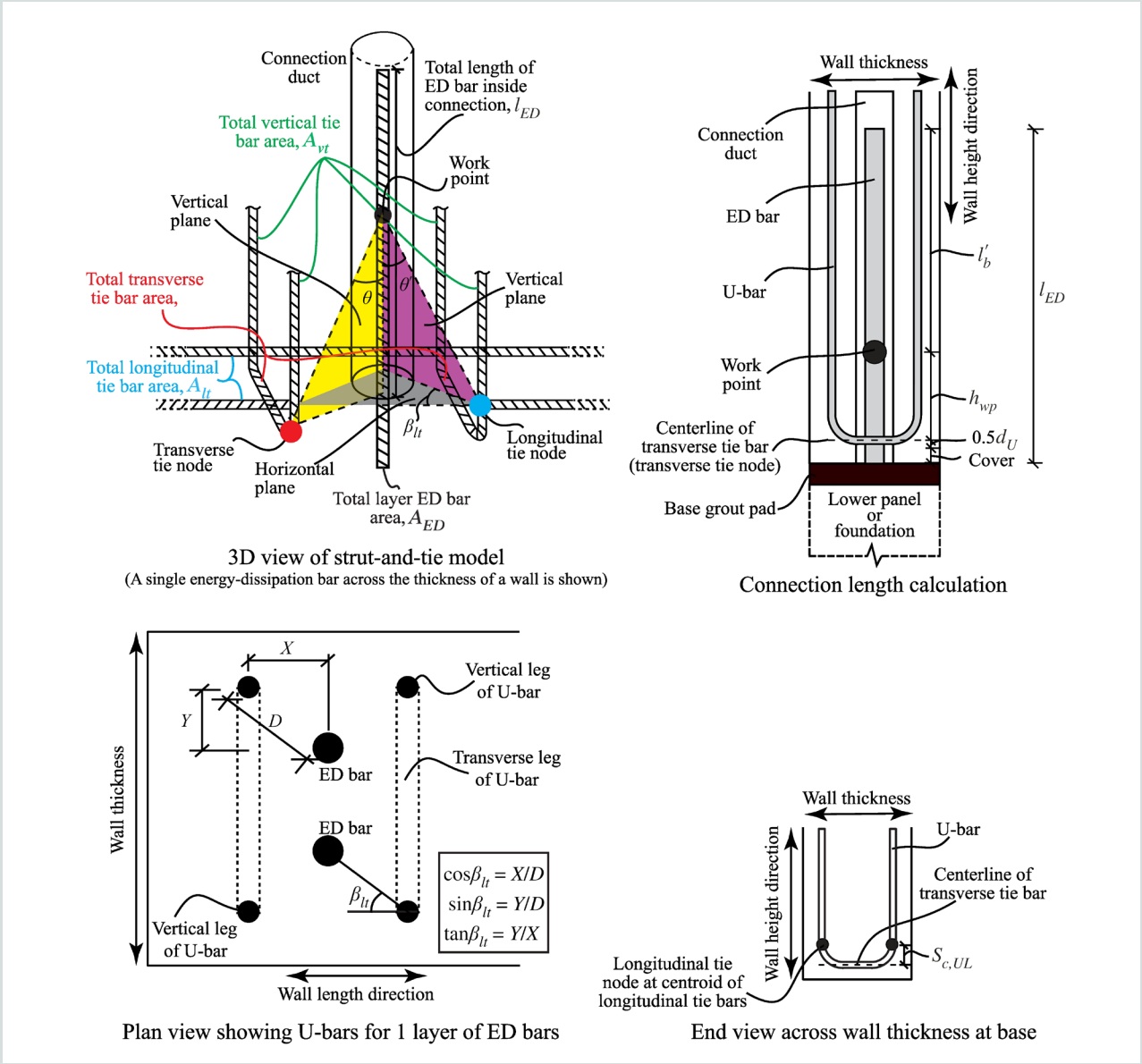

Figure 1. Strut-and-tie model. Note: A_{ED} = total area of energy-dissipation bar or bars in one layer across thickness of wall cross section; A_{lt} = total required area of longitudinal tie reinforcement to transfer tension force in A_{ED}; A_{tt} = total required area of transverse tie reinforcement to transfer tension force in A_{ED}; d_U = diameter of U bar; D = horizontal distance between center of energy-dissipation reinforcing bar and center of vertical tie bar (vertical leg of U bar); ED = energy-dissipation; h_{wp} = height of strut-and-tie model work point measured from center of transverse tie (horizontal leg of U bar) projected onto energy-dissipation bar; l'_b = prescribed grouted bond length extension (beyond strut-and-tie work point) of 9 times bar diameter for no. 7, 8, and 9 (22M, 25M, and 29M) energy-dissipating bars and 12 times bar diameter for no. 10 and 11 (32M and 36M) bars; l_{ED} = length of energy-dissipation bar inside connection duct; $S_{c,UL}$ = vertical distance between center of transverse tie bar (horizontal leg of U bar) and centroid of longitudinal tie reinforcement; X = horizontal distance between center of energy-dissipation reinforcing bar and center of vertical tie bar (vertical leg of U bar) in wall length direction; Y = horizontal distance between center of energy-dissipation reinforcing bar and center of vertical tie bar (vertical leg of U bar) in wall thickness direction; β_{lt} = horizontal plane angle of strut-and-tie model (complementary to β_{tt}); β_{tt} = horizontal plane angle of strut-and-tie model (complementary to β_{lt}); θ = vertical plane angle of strut-and-tie model between work point and transverse tie node; θ' = vertical plane angle of strut-and-tie model between work point and longitudinal tie node.

the base of the wall panel into ducts cast inside the top of the foundation (the connection would be rotated vertically 180 degrees, as compared with the depiction in Fig. 1).

The design intent is for the vertical tie reinforcing bars to yield when the energy-dissipation bars yield, while the transverse and longitudinal tie reinforcing bars do not yield until the ultimate (peak) strength of the energy-dissipation bars is reached. These design choices are made to spread the yielding of flexural reinforcement into the wall panel (and reduce concentration of yielding at the horizontal joint) while limiting the amount of vertical cracking of the wall panel around the

connections so that the concrete can provide effective confinement to the connection ducts.

Based on Al-Khateeb et al.,[6] the required (minimum) vertical tie reinforcement area for the connection is calculated using vertical equilibrium of the strut-and-tie model, given in Eq. (1).

$$A_{vt} = \frac{A_{ED} \times f_{y,ED}}{f_{y,vt}} \quad (1)$$

where

A_{vt} = total area of vertical tie reinforcement required to transfer the force in A_{ED} across the connection

A_{ED} = total area of the energy-dissipation bar or bars placed in one layer across the thickness of the wall

$f_{y,ED}$ = yield strength of the energy-dissipation bars

$f_{y,vt}$ = yield strength of the vertical tie bars

Validation of the short-grouted connections in this research project was limited to ASTM A706[10] Grade 60 (414 MPa) reinforcing steel. Therefore, $f_{y,vt} = f_{y,ED} = 60$ ksi, and Eq. (1) can be simplified as follows in Eq. (2):

$$A_{vt} = A_{ED} \quad (2)$$

Using U bars for the vertical tie reinforcement is a prescribed, mandatory design requirement based on the shear wall tests described in Al-Khateeb et al.[5] The horizontal legs of these U bars serve as the connection transverse tie reinforcement. Thus, the total vertical leg area of the U bars dictates the reinforcement area for the transverse ties as given by Eq. (3).

$$A_{tt} = \frac{A_{vt}}{2} \quad (3)$$

where

A_{tt} = total area of the transverse tie reinforcement used to transfer the force in A_{ED} across the connection

Using nodal force equilibrium of the strut-and-tie model, Eq. (4) through (6) were derived in Al-Khateeb et al.[6] to determine the total longitudinal tie area A_{lt} required to transfer the force in A_{ED} across the connection.

$$A_{lt} = \frac{A_{vt}}{2} \times R \times \tan\left(\theta'\right) \times \cos\left(\beta_{lt}\right) \quad (4)$$

$$\tan\left(\theta'\right) = \frac{D}{h_{wp} - S_{c,UL}} \text{ for } 25 \le \theta' \le 65 \quad (5)$$

$$\cos\left(\beta_{lt}\right) = \frac{X}{D} \text{ for } 25 \le \beta_{lt} \le 65 \quad (6)$$

where

R = ratio between the ultimate (peak) strength of the vertical tie reinforcing steel $f_{u,vt}$ and the yield strength of the longitudinal tie reinforcing steel $f_{y,lt}$

θ' = vertical plane angle of the strut-and-tie model between the work point and the longitudinal tie node

β_{lt} = horizontal plane angle of the strut-and-tie model

D = horizontal distance between the center of the energy-dissipation bar and center of the vertical tie bar (vertical leg of the U bar)

h_{wp} = height of the work point measured from the center of the transverse tie (horizontal leg of the U bar) projected onto the energy-dissipation bar

$S_{c,UL}$ = vertical distance between the center of the transverse (horizontal) leg of the U bar and the centroid of the longitudinal tie reinforcement on each face of the wall (Fig. 1)

X = horizontal distance between the center of the energy-dissipation bar and center of the vertical tie bar (vertical leg of the U bar) in the wall length direction (Fig. 1)

Substituting Eq. (2), (5), and (6) into Eq. (4) and taking R as 1.5 for ASTM A706[10] Grade 60 (414 MPa) reinforcing bars results in Eq. (7).

$$A_{lt} = \frac{0.75 \times X}{h_{wp} - S_{c,UL}} \times A_{ED} \quad (7)$$

The longitudinal tie reinforcement should be placed close to the transverse (horizontal) legs of the U bars such that Eq. (8) is satisfied.

$$S_{c,UL} < h_{wp} \quad (8)$$

As discussed later, increased distance between the centroid of the longitudinal tie bars and the transverse legs of the U bars (that is, increased $S_{c,UL}$) will result in a longer grouted connection length.

The strut-and-tie model angles θ' and β_{lt} in Fig. 1 depend on the layout of the tie reinforcement and energy-dissipation bars in the wall (or foundation) cross section, expressed in terms of the X and Y dimensions per Eq. (5) and (6), where Y is the horizontal distance between the center of the energy-dissipation bar and center of the vertical tie bar (vertical leg of the U bar) in the wall thickness direction. (Note that $X^2 + Y^2 = D^2$ based on the Pythagorean theorem.) Although θ' and β_{lt} are eliminated in Eq. (7), these angles must satisfy the maximum and minimum strut-and-tie angle limits specified in ACI 318-19[8] section 23.2.7, as described by Eq. (9) and (10).

$$\left(\left(\tan 25\right) = 0.47\right) \le \left(\tan\left(\theta'\right) = \frac{D}{h_{wp} - S_{c,UL}}\right) \le \left(\left(\tan 65\right) = 2.1\right) \quad (9)$$

$$\left(\left(\cos 65\right) = 0.42\right) \le \left(\cos\left(\beta_{lt}\right) = \frac{X}{D}\right) \le \left(\left(\cos 25\right) = 0.91\right) \quad (10)$$

As given in Eq. (11), the limits for θ' and β_{lt} can be combined into conservative upper and lower limits for the term $\tan(\theta') \times \cos(\beta_{lt})$ in Eq. (4). Specifically, when θ' is limited to 65 degrees, β_{lt} can be assumed to be equal to 25 degrees as the upper bound, and when β_{lt} is limited to 65 degrees, θ' can be assumed to be equal to 45 degrees as the lower bound.

$$\left(\left(\tan 45\right)\times\left(\cos 65\right)=0.42\right)\le\left(\left(\tan\left(\theta'\right)\right)\times\left(\cos\left(\beta_{lt}\right)\right)=\frac{D}{h_{wp}-S_{c,UL}}\times\frac{X}{D}\right)\le\left(\left(\tan 65\right)\times\left(\cos 25\right)=2.0\right)\rightarrow$$

$$0.42\le\frac{X}{h_{wp}-S_{c,UL}}\le 2.0 \tag{11}$$

These simplifications to determine upper and lower limits for the term $\tan(\theta') \times \cos(\beta_{lt})$ were made after analyzing the effects of changing the connection reinforcement layout (as quantified by X and Y) on the strut-and-tie model angles θ' and β_{lt}. **Figure 2** shows how an increase in the X dimension (for example, from X_1 to X_2) results in an increase in θ' (from θ'_1 to θ'_2) and a decrease in β_{lt} (from β_{lt1} to β_{lt2}). Conversely, an increase in Y (for example, from Y_1 to Y_2 in Fig. 2) causes an increase in the height of the work point h_{wp} (per Eq. [17], discussed later), which results in a decrease in θ' and an increase in β_{lt}. The three-dimensional plots in Fig. 2 demonstrate the inverse relationship between θ' and β_{lt} for X and Y varying within a range of 2 to 5 in. (51 to 127 mm). Specifically, these plots reveal that θ' consistently reaches its maximum limit of 65 degrees (per ACI 318-19 section 23.2.7) before β_{lt} reaches its minimum limit of 25 degrees. Consequently, limiting β_{lt} to 25 degrees when θ' is capped at 65 degrees provides a conservative and efficient design approach for checking these limits, resulting in the upper bound limit of 2.0 for the term $\tan(\theta') \times \cos(\beta_{lt})$ in Eq. (11).

In comparison, as β_{lt} reaches its maximum limit of 65 degrees (per ACI 318-19[8] section 23.2.7), θ' approaches 45 degrees, which is greater than the ACI 318-19 minimum limit of 25 degrees. This finding demonstrates that the ACI 318-19 minimum limit of 25 degrees for θ' will not be reached. Instead, based on the results in Fig. 2, a conservative value of $\theta' = 45$ degrees was selected for the calculation of the lower-bound limit of 0.42 in Eq. (11).

Finally, the required (minimum) area of longitudinal tie reinforcement can be determined by applying the limits in Eq. (11) to Eq. (7) as follows:

$$0.32\times A_{ED}\le A_{lt}=\frac{0.75\times X}{h_{wp}-S_{c,UL}}\times A_{ED}\le 1.5\times A_{ED} \tag{12}$$

In Eq. (12), $\frac{0.75\times X}{h_{wp}-S_{c,UL}}$ is referred to as the longitudinal tie reinforcement area multiplier K as defined in Eq. (13).

$$0.32\le K=\frac{0.75\times X}{h_{wp}-S_{c,UL}}\le 1.5 \tag{13}$$

The height of the work point h_{wp} is derived in Al-Khateeb et al.[6] as follows:

$$h_{wp}=R\times Y \tag{14}$$

Per Eq. (5), θ' depends on the location of the work point and should be between 25 and 65 degrees. Figure 2 shows that θ' does not reach the lower limit of 25 degrees and only the upper limit of 65 degrees can control design. The height of the work point corresponding to this upper limit can be derived from Eq. (5) as follows in Eq. (15) and (16):

$$h_{wp}=\frac{D}{\tan\left(65\right)}+S_{c,UL} \tag{15}$$

$$h_{wp}=0.5\sqrt{X^2+Y^2}+S_{c,UL} \tag{16}$$

In addition, if h_{wp} calculated using Eq. (14) is less than or equal to $S_{c,UL}$, then the location of the work point should be moved up to create an angle of 65 degrees with the longitudinal tie node, satisfying the upper limit of θ'. These limitations for calculating h_{wp} can be combined in Eq. (17), with R in Eq. (14) taken as 1.5 for ASTM A706[10] Grade 60 (414 MPa) reinforcing bars.

$$h_{wp}=\begin{cases}1.5\times Y\ge 0.5\sqrt{X^2+Y^2}+S_{c,UL} & \text{if } S_{c,UL}<1.5\times Y\\ 0.5\sqrt{X^2+Y^2}+S_{c,UL} & \text{if } S_{c,UL}\ge 1.5\times Y\end{cases} \tag{17}$$

The total required (minimum) area of longitudinal tie reinforcement A_{lt} given in Eq. (12) is a function of both the total area A_{ED} of the energy-dissipation bar or bars placed in one layer across the thickness of the wall and the layout of the tie reinforcement around the connections (X, Y, and $S_{c,UL}$). **Figure 3** illustrates the effect of different tie reinforcement arrangements on K for $S_{c,UL}$ values of 1.5, 2.5, and 3.0 in. (38, 64, and 76 mm). Increasing the X dimension increases K because the vertical legs of the U bars are placed farther apart from the energy-dissipation bars along the wall length, requiring a larger longitudinal tie reinforcement area A_{lt} to achieve equilibrium in the strut-and-tie model. Conversely, increasing the Y dimension decreases the multiplier but increases the height of the work point h_{wp} (Eq. [17]), which also increases the connection length, as described later.

Based on the observed damage in shear wall specimen 2 described in Al-Khateeb et al.,[5] the longitudinal tie bars should engage the U bars, and the centroid of the longitudinal tie bars should be placed as close as possible to the transverse (horizontal) legs of the U bars. Placing the longitudinal tie bars in multiple layers over the length of the connection ducts (that is, over the height of the wall) moves the centroid of these bars away from the transverse legs of the U bars, thus increasing $S_{c,UL}$. This reduces the effectiveness of the longitudinal tie bars and leads to an increase in the longitudinal tie area multi-

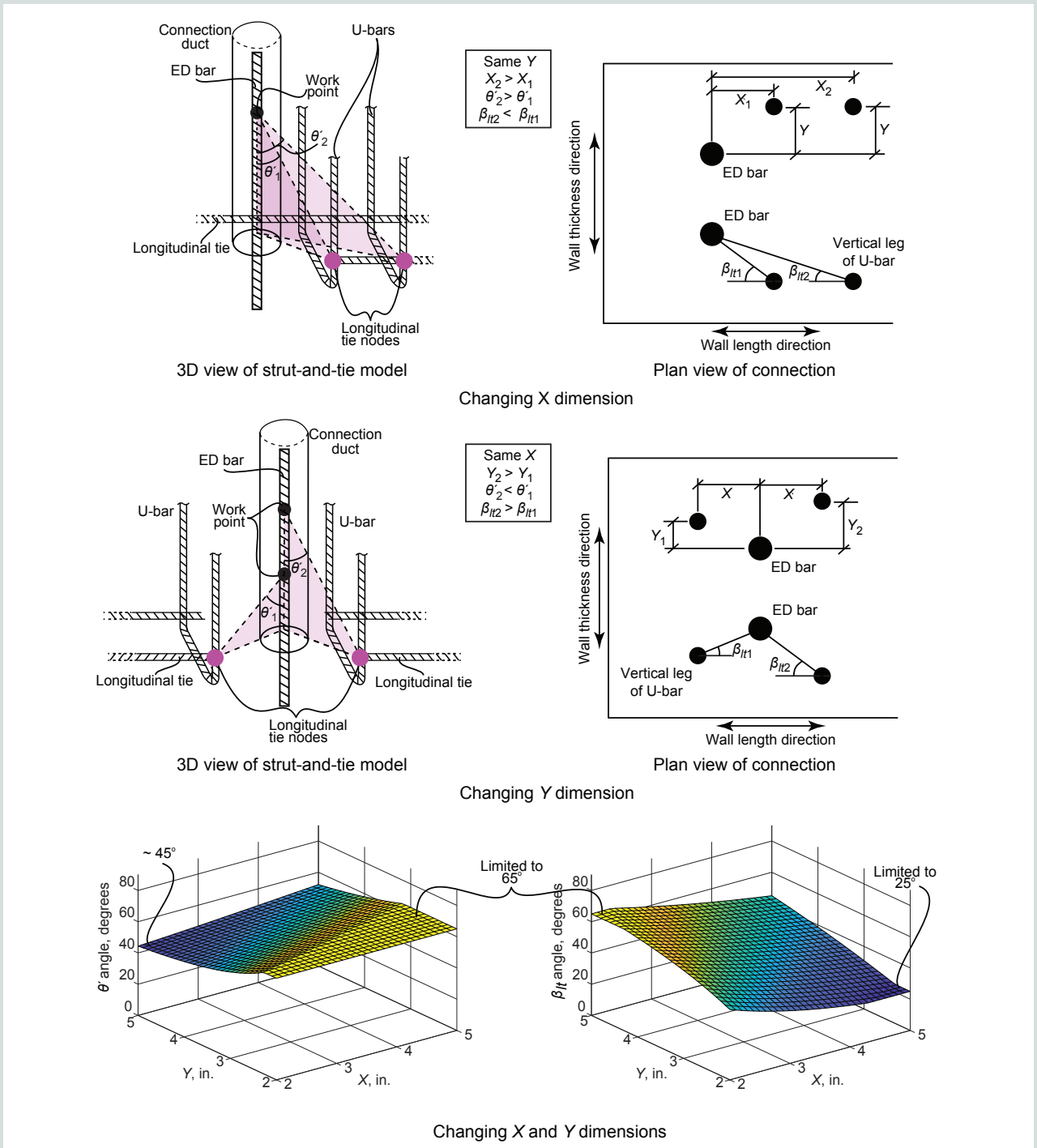

Figure 2. Effect of X and Y dimensions on strut-and-tie angles θ' and β_{lt}. Note: ED = energy-dissipation; X = horizontal distance between center of energy-dissipation reinforcing bar and center of vertical tie bar (vertical leg of U bar) in wall length direction; X_1 = horizontal distance between center of energy-dissipation reinforcing bar and center of vertical tie bar (vertical leg of U bar) in wall length direction, sample 1; X_2 = horizontal distance between center of energy-dissipation reinforcing bar and center of vertical tie bar (vertical leg of U bar) in wall length direction, sample 2; Y = horizontal distance between center of energy-dissipation reinforcing bar and center of vertical tie bar (vertical leg of U bar) in wall thickness direction; Y_1 = horizontal distance between center of energy-dissipation reinforcing bar and center of vertical tie bar (vertical leg of U bar) in wall thickness direction, sample 1; Y_2 = horizontal distance between center of energy-dissipation reinforcing bar and center of vertical tie bar (vertical leg of U bar) in wall thickness direction, sample 2; β_{lt} = horizontal plane angle of strut-and-tie model (complementary to β_{tt}); β_{lt1} = horizontal plane angle of strut-and-tie model (complementary to β_{tt}), sample 1; β_{lt2} = horizontal plane angle of strut-and-tie model (complementary to β_{tt}), sample 2; θ' = vertical plane angle of strut-and-tie model between work point and longitudinal tie node; θ'_1 = vertical plane angle of strut-and-tie model between work point and longitudinal tie node, sample 1; θ'_2 = vertical plane angle of strut-and-tie model between work point and longitudinal tie node, sample 2. 1 in. = 25.4 mm.

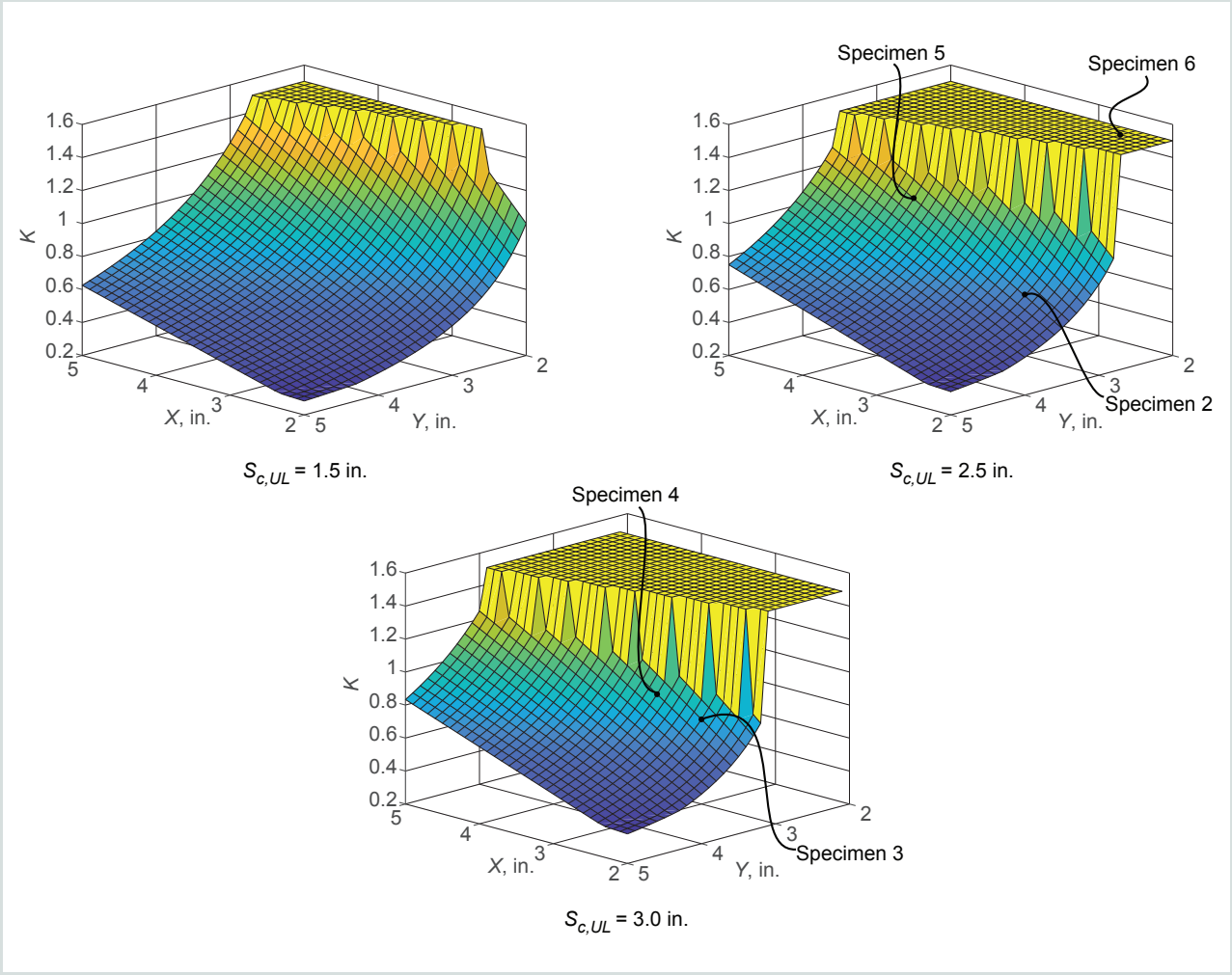

Figure 3. Effect of arrangement of tie reinforcement on longitudinal tie reinforcement area multiplier *K*. Note: $S_{c,UL}$ = vertical distance between center of transverse tie bar (horizontal leg of U bar) and centroid of longitudinal tie reinforcement; *X* = horizontal distance between center of energy-dissipation reinforcing bar and center of vertical tie bar (vertical leg of U bar) in wall length direction; *Y* = horizontal distance between center of energy-dissipation reinforcing bar and center of vertical tie bar (vertical leg of U bar) in wall thickness direction. 1 in. = 25.4 mm.

plier *K*, eventually triggering the upper limit value of 1.5 in Eq. (13), which is shown in Fig. 3 for different values of $S_{c,UL}$. Longitudinal tie reinforcement areas above this upper limit of $1.5 \times A_{ED}$ are ineffective and should not be included in the connection design. While it is permissible to design a connection where the longitudinal tie reinforcement area is limited to the upper-bound value of $1.5 \times A_{ED}$, this detail will result in an increase in $S_{c,UL}$ and the height of the work point h_{wp}—per Eq. (15), (16), and (17)—and subsequently lead to an increase in the connection length (described later).

Figure 3 shows the required longitudinal tie reinforcement area multiplier *K* for each shear wall specimen tested in this research, except for specimen 1,[5] which did not use U bars as the vertical and transverse tie reinforcement, rendering it outside the intent of the design recommendations herein. Specimen 2 used a single layer of longitudinal tie bars; however, the placement of these bars was inefficient (the longitudinal tie bars were placed away from the transverse legs of the U bars),[5] resulting in an $S_{c,UL}$ value of 2.50 in. (64 mm), which contributed (among other factors[5]) to the insufficient performance of that specimen to satisfy ACI 550.6-19.[7] Specimen 3 used two layers of longitudinal tie bars. The first layer of these bars was placed at 2.00 in. (51 mm) from the transverse legs of the U bars, resulting in only a slight increase in $S_{c,UL}$ to a value of 2.94 in. (75 mm). The closer placement of the first layer of longitudinal tie bars to the transverse legs of the U bars, along with other design and detailing modifications,[5] improved the confinement and force transfer of the connection at the wall base. As described in Al-Khateeb et al.,[5] this wall satisfied the applicable performance requirements specified by ACI 550.6-19.

Two layers of longitudinal tie bars were used in specimens 4, 5, and 6, with $S_{c,UL}$ values of 2.88, 2.75, and 2.56 in. (73, 70, and 65 mm), respectively. The first layer of longitudinal tie bars was placed as close as possible to the transverse legs of the U bars, but the longitudinal tie reinforcement areas

for specimens 4 and 5 were calculated prior to the development of the final strut-and-tie design procedure described in this paper. Specifically, the longitudinal tie reinforcement areas for specimens 4 and 5 were calculated by lumping (for design purposes) all of the longitudinal reinforcement at the first layer, resulting in smaller $S_{c,UL}$ values (2.06 and 1.81 in. [52 and 46 mm], respectively). This simplification led to slightly under-designed longitudinal tie reinforcement areas in these walls; in specimen 4, these bars yielded by the end of the test.[6] Despite using slightly smaller longitudinal tie reinforcement areas compared with the areas required by the subsequently revised strut-and-tie model, the overall performance of both specimens 4 and 5 satisfied ACI 550.6-19, with no significant concrete damage, indicating good confinement and force transfer around the connections. The longitudinal tie reinforcement area of specimen 6 was determined according to the procedure described herein and was limited to the upper bound of $1.5 \times A_{ED}$. This specimen demonstrated satisfactory performance as well and also showed no yielding of the longitudinal ties throughout the test, which was consistent with the aforementioned design intent, indicating that the reinforcement was not under-designed.

The last step in the short-grouted connection design is determining the required (minimum) connection length l_{ED} (that is, the minimum embedment length of the energy-dissipation bars inside the connection ducts), given in Eq. (18) from Al-Khateeb et al.[6] as follows:

$$l_{ED} = C + 0.5 \times d_U + h_{wp} + l'_b \quad (18)$$

where

C = clear vertical cover to the U bars

d_U = U bar diameter

l'_b = prescribed minimum grouted bond length extension (beyond the strut-and-tie model work point) of nine times the bar diameter ($9d_{ED}$) for no. 7, 8, and 9 (22M, 25M, and 29M) energy-dissipating bars and $12d_{ED}$ for no. 10 and 11 (32M and 36M) bars

Note that only specimens with no. 7, 9, and 11 energy-dissipation bars were tested in this research. The aforementioned minimum bond length extension recommendations for no. 8 and 10 bars are based on the specimens with no. 9 and 11 bars, respectively.

Wall shear design and special boundary confinement reinforcement are outside the scope of this paper. However, this reinforcement should be considered when placing the connection ducts and tie reinforcement in the wall cross section. The longitudinal tie reinforcement should not be included in the shear reinforcement ratio when determining the nominal shear strength of the wall. The first shear reinforcing bar at the bottom of the wall should be placed above all of the longitudinal tie reinforcement for the connection or its area should be added to the longitudinal tie reinforcement area.

Connection detailing

Key connection detailing recommendations were developed based on the experimental program of this research project. These recommendations, combined with the connection design procedure derived from the strut-and-tie model, resulted in ductile performance of the shear wall specimens that were tested.[5,6]

One important detail is the use of U bars around the connection ducts, where the vertical legs of the U bars serve as vertical tie reinforcement and the transverse (horizontal) legs serve as transverse tie reinforcement. This detail was implemented after testing specimen 1, which used headed bars for the vertical tie reinforcement and separate rectilinear bars as the transverse tie reinforcement.[5] The headed bars were ineffective in transferring the energy-dissipation bar forces to the wall, resulting in premature failure due to breakout of the connection group at each end of the wall. Subsequent testing of specimens 2 through 6 demonstrated that using U bars around the connection ducts significantly improved the performance of the walls.[5,6]

Smaller diameter U bars should be selected to minimize their bend radius and accommodate more efficient placement of the tie reinforcement around the connection ducts. However, when desirable, the required U bar areas for two adjacent layers (over the wall length) of energy-dissipation bars can be combined, as discussed in Al-Khateeb et al.[5] This detail was implemented in specimen 4,[6] where a pair of no. 5 (16M) U bars designed as the vertical and transverse ties between two layers of energy-dissipation bars were combined into a single no. 7 (22M) U bar. The U-bar bend radii for the connections in all test specimens satisfied the minimum bend radii specified for ties in Table 25.3.2 of ACI 318-19. Note that this research was informed by strut-and-tie design principles but did not consider all of the strut-and-tie design details of ACI 318-19, such as section 23.10 for curved bar nodes, in an effort to provide a practical design methodology. The provided bend radii for the U bars in specimens 3, 4, and 5 were larger than those calculated using ACI 318-19 Eq. (23.10.2b) and section 23.10.3 for 180-degree bends, while the U bars in specimen 6 had smaller 180-degree bend radii. No differences were observed in the performance of the strut-and-tie nodal zones between these specimens.

ASTM A706[10] Grade 60 (414 MPa) bars should be used for the transverse ties (U bars) and longitudinal ties to effectively confine the concrete and transfer forces around the connection ducts. Specifically, compared with higher-grade steel, using Grade 60 bars increases the minimum required areas of horizontal (that is, transverse and longitudinal) tie reinforcement, which helps control the development of vertical cracks around the connection ducts.

The vertical legs of the U bars should be fully developed beyond the end of the energy-dissipation bars, ensuring that the minimum required length of the vertical legs of the U bars l_U is the sum of the connection length l_{ED}, calculated using

Eq. (18), and the development length l_d of the U bar, calculated using ACI 318-19[8] section 25.4.2. Where providing the full l_U is not feasible, such as in the case of connections placed inside a shallow foundation, the vertical legs of the U bars can be hooked or headed, providing an adequate development length in accordance with ACI 318-19 section 25.4.3 or 25.4.4, respectively, beyond the end of the energy-dissipation bars. For connections placed inside a wall panel, the U bars can serve as the vertical panel reinforcement or can be lap spliced with the vertical panel reinforcement.

Another important detail is the intentional unbonding (by wrapping inside plastic sheathing) of the energy-dissipation bars over a length of $3d_{ED}$ inside the connection ducts (that is, within the connection length l_{ED}) and immediately adjacent to the precast concrete joint (**Fig. 4**). This unbonding detail helps reduce the tension demands in the concrete at the beginning of the connection by transferring the energy-dissipation bar forces to a region of the wall where the concrete is better confined by the reinforcement. This detailing was introduced after testing specimen 2,[5] which suffered from severe concrete damage at the bottom of the wall due to the high localized connection forces and was adopted based on the recommendations of Barbachyn et al.[11] for flexural reinforcement in the boundary regions of special reinforced concrete shear walls. The observed behaviors of specimens 3 through 6[5,6] confirmed that the intentional unbonding of the energy-dissipation bars improved the connection performance and reduced the damage concentrated at the bottom of the walls. In addition to the $3d_{ED}$ unbonded length, the energy-dissipation bars should also be intentionally unbonded within the horizontal joint grout pad to limit damage to the grout pad by transferring the bar forces above and below the pad rather than within the pad. The plastic wrap material used for unbonding should be secured onto the bars so that the unbonded location does not shift during construction. Furthermore, the plastic wrap should be thick enough to create a smooth cover over the bar ribs (lugs) so that mechanical interlock with the surrounding grout is prevented, but not excessively thick so that the bars can still provide dowel resistance across the precast concrete joint. Plastic window insulation tape, 0.024 in. (0.61 mm) thick, was used as the unbonding material for the energy-dissipation bars in this research.

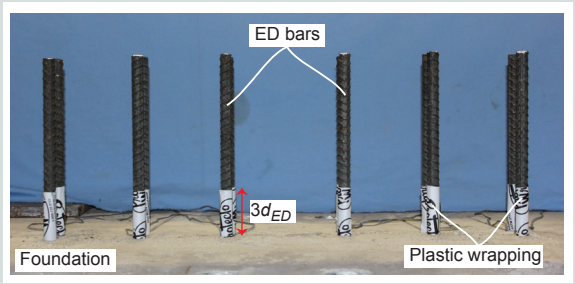

Figure 4. Intentional unbonding of energy-dissipation bars. Note: d_{ED} = diameter of energy-dissipation bar; ED = energy-dissipation.

As shown in **Fig. 5**, the first layer of reinforcing steel around the connections should be placed as close to the precast concrete joint as possible, while complying with the minimum concrete cover requirements of ACI 318-19[8] section 20.5.1. This recommendation applies to the transverse legs of the U bars and the concrete confinement reinforcement (hoops and ties) in special boundary elements. Minimizing the concrete cover enhances the effectiveness of confinement around the connection ducts, as demonstrated in specimens 3 through 6, which used 0.75 in. (19 mm) concrete cover to the steel reinforcement. In contrast, specimen 2, which had a larger (1.5 in. [38 mm]) concrete cover, exhibited more damage adjacent to the joint, as discussed in Al-Khateeb et al.[5]

The centroid of the longitudinal tie bars should be placed as close as possible to the transverse legs of the U bars (Fig. 5) to minimize $S_{c,UL}$, thereby reducing the required longitudinal tie reinforcement area A_{lt}, as discussed in the connection

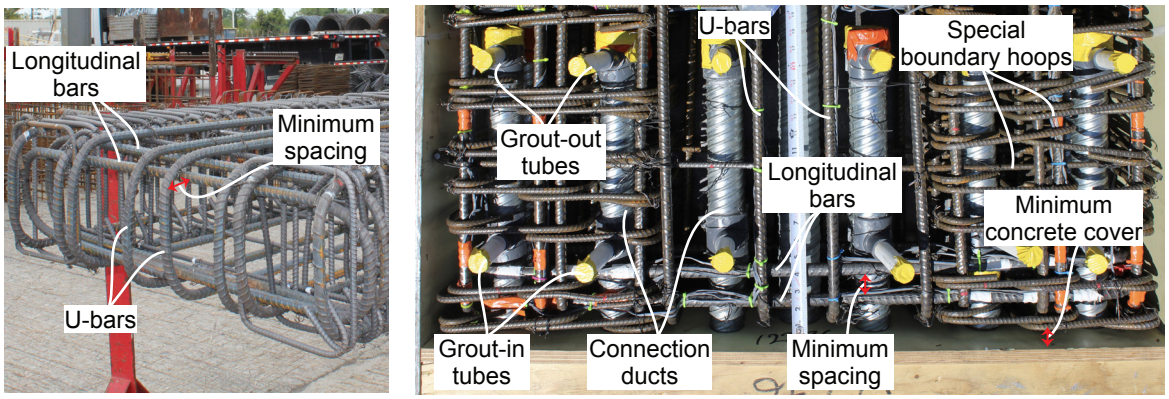

Figure 5. Placement of reinforcement around connection ducts.

design section of this paper. If the longitudinal tie reinforcement is provided by a single layer of bars over the connection length, then the centerline of each bar should be placed no closer to the transverse legs of the U bars than the center half of the U-bar bend. The intent of this requirement is to ensure that the longitudinal tie bars engage the U bar. If the longitudinal tie reinforcement is provided in multiple layers (Fig. 5), the clear spacing between the layers should comply with the minimum spacing requirements of ACI 318-19 section 25.2. Minimizing the spacing between layers of longitudinal tie bars reduces $S_{c,UL}$, consequently reducing A_{lt}.

The longitudinal tie reinforcement should be fully developed along the connection region and anchored at the wall ends. Where connection ducts are distributed along the wall length, the longitudinal tie bars can be developed by providing them as closed hoops around the full wall length or as horizontal U bars placed at each end and spliced along the wall length. Where connections are used only at the wall ends, closed hoops can be placed around each connection group or horizontal U bars can be used at each end of the wall with full development length (calculated per ACI 318-19[8] section 25.4.2) beyond the last (innermost) connection layer. For connections placed inside the foundation, the longitudinal bars can be developed as continuous straight bars that extend beyond the outermost layer of connection ducts at each end.

Commercially available prebagged nonshrink cementitious grout in pumpable consistency should be used for the connection grout of the energy-dissipation bars. The grout pad needed for construction tolerances and alignment at the horizontal joint between the wall and the foundation (as well as any upper panel-to-panel joint grout pad) should also be constructed using nonshrink cementitious grout. To ensure proper integrity of the grout, the grout placement at each location should be completed in a single application. The base joint grout pads of the test specimens in this research program were constructed using two different methods:

- The wall panel was lowered on top of 1 in. (25 mm) thick wooden shims placed inside freshly mixed grout in a plastic consistency per the grout manufacturer's recommendations.

- The wall panel was aligned on top of 1 in. (25 mm) thick wooden shims, and grout mixed in a pumpable consistency according to manufacturer's recommendations was manually spread and pumped under the wall.

Either of these methods can be used to ensure that the grout pad is free of voids and defects, but the second method was easier to apply and achieved more consistent results for the construction of the base joint grout pads in this research. The horizontal joint grout pads should be of adequate thickness (approximately 1 in. [25 mm]) for the chosen method of construction. The integrity of the grout at joints where nonlinear behavior of the wall is expected has significant importance for the seismic performance of the wall. To limit deterioration of the grout pad during the lateral displacements of the wall subjected to a large earthquake, polypropylene fibers (dosage per the fiber manufacturer) should be added to the grout mixture at these joints. Dry packing of this grout is not recommended because it would be difficult to ensure that the grout is adequately compacted without voids over the entire joint volume with this method. ACI 550.7-19[12] requires the nonshrink base pad grout at the wall–foundation joint interface to contain at least 0.1% fibers by volume and the thickness of this grout not to exceed 1.5 in. (38 mm) in order to prevent failure of the grout pad under combined shear and axial stresses.

On wall test day, the compression strengths of the connection grout for the specimens that passed the ACI 550.6-19[7] validation requirements were as follows: 8.52 ksi (58.7 MPa) for specimen 3, 9.88 ksi (68.1 MPa) for specimen 4, 9.68 ksi (66.7 MPa) for specimen 5, and 8.75 ksi (60.3 MPa) for specimen 6.[5,6] The base joint pad grout strengths for the same specimens were 11.3, 9.45, 8.32, and 8.59 ksi (77.9, 65.1, 57.4, and 59.2 MPa), respectively. Based on these results, a minimum 28-day compression strength of 9.00 ksi (62.1 MPa) should be specified for both the connection grout and the joint pad grout. ACI 550.7-19[12] requires the specified compression strength of the joint pad grout not to be less than the specified compression strength of the adjacent precast concrete wall panel. In addition, it recommends the compression strength of the joint pad grout to be close to the compression strength of the wall panel to provide a matching (with compatible strength) bearing bed for the wall at large lateral displacement levels.

The location of the connection ducts dictates the connection grout placement method. If the energy-dissipation bars protrude down from the bottom of a wall panel, grout can be pumped or gravity-placed into the ducts located at the top of the lower panel or foundation before or after lowering the upper panel into position, ensuring that the entire duct is filled with grout without air pockets. If instead the energy-dissipation bars protrude up from the top of a lower wall panel or foundation, grout-in and grout-out tubes must be attached to the connection ducts inside the upper panel to facilitate grout pumping without air pockets. It is important to ensure that the grout pad at the horizontal joint immediately below the connection ducts fully seals the connection grout from leaking out of the ducts. The grout-in tube locations should be specified in the wall panel shop drawings and should be positioned above the first reinforcement layer (special boundary confinement hoops and transverse legs of U bars), as illustrated in **Fig. 6**. This detailing was introduced after testing specimen 2, which had grout-in tubes located below the first layer of connection reinforcement, resulting in this reinforcement being placed farther away from the precast concrete joint. The grout-out tube locations should also be specified and be placed at least 1 in. (25 mm) above the end of the energy-dissipation bar to ensure that the full length of the bar is grouted.

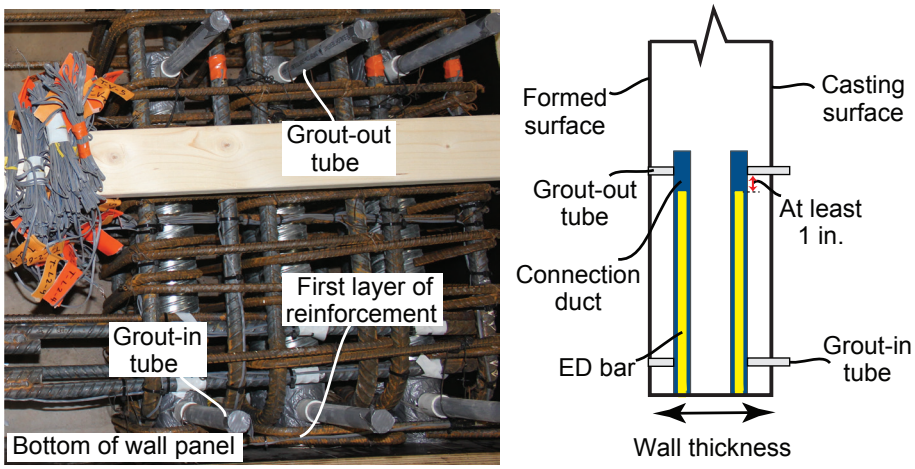

Figure 6. Grout-in and grout-out tubes. Note: ED = energy-dissipation. 1 in. = 25.4 mm.

Straight corrugated steel ducts (**Fig. 7**), commonly used in post-tensioning applications in the construction industry, can serve as connection ducts if they have sufficient thickness and corrugations. A minimum steel thickness of 0.018 in. (0.46 mm) (26 gauge) is recommended, as the ducts used in this experimental program were all 26 gauge. Because corrugation patterns differ among duct manufacturers, the recommended minimum amount of corrugation is expressed as a cumulative corrugation depth, calculated as the number of corrugations per foot of duct multiplied by the nominal corrugation depth. Based on the ducts used in the wall test specimens that passed the ACI 550.6-19[7] validation requirements, a minimum cumulative corrugation depth of 1.25 in./ft (104 mm/m) is recommended. The cumulative corrugation depth for the ducts used in specimen 3 was 1.72 in./ft (143 mm/m), while for specimens 4, 5, and 6, it was 1.25 in./ft.

The inner diameter of the connection ducts d_{duct} should be 1 to 2 in. (25 to 51 mm) larger than the nominal diameter of the energy-dissipation bars d_{ED} to provide sufficient placement and grouting tolerance around the energy-dissipation bars (Fig. 7). Excessively small ducts could cause erection and installation challenges and impede effective grout placement. Excessively large connection ducts should also be avoided, as their use could complicate detailing and fabrication by increasing the distance between adjacent energy-dissipation bars. This is particularly important for connections placed inside a thin wall panel, where the limited wall thickness must accommodate the connection ducts, tie reinforcement, and special boundary confinement hoops with adequate concrete cover. Each connection duct should extend a few inches beyond the end of the energy-dissipation bar to allow for installation tolerances and accommodate the placement of the grout-out tube (when grout is pumped into ducts at the bottom of a wall panel).

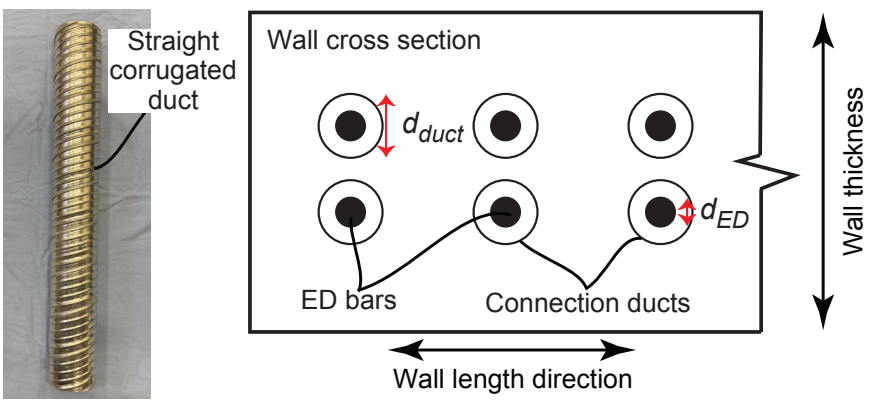

Figure 7. Connection ducts. Note: d_{duct} = diameter of connection duct; d_{ED} = diameter of energy-dissipation bar; ED = energy-dissipation.

Fiber-element nonlinear numerical modeling and analysis

A two-dimensional fiber-element numerical model was developed using the Open System for Earthquake Engineering Simulation (OpenSees) platform to analyze the reversed-cyclic nonlinear lateral-load behavior of the precast concrete wall specimens tested as part of this research project.[5,6] The numerical model used conventional techniques commonly adopted for the analysis of reinforced concrete shear walls and was refined and validated based on the measured behaviors of the test specimens. Each specimen was modeled using a single force-based beam-column element representing the height of the wall (**Fig. 8**). The top node of the element was at the location of the lateral-load application, while the bottom node was at the top of the base grout pad. The height of the specimen above the lateral-load application point was not modeled. For specimens 4 through 6, the increased wall length to accommodate the lateral-load actuator-to-wall connection at the top was also not modeled, resulting in a constant wall length over the entire height of each numerical model. The top node was free to displace, while the bottom node was fixed, without modeling the grout base pad or the foundation. Five integration points with the Gauss-Lobatto integration method were used along the height of the fiber element.[13] The nonlinear axial-flexural behavior of the wall was modeled using a number of uniaxial fibers (oriented along the wall height) with assigned nonlinear material properties for the concrete and the energy-dissipation bars (**Fig. 9**). No other reinforcement was explicitly modeled, and the shear behavior of the wall was assumed to be linear elastic. The analyses were conducted under displacement control following the applied lateral loads and displacements during each test, together with the applied superimposed axial load and the self-weight of the wall (Fig. 8). Only one cycle of loading was applied at each lateral displacement increment, with the exception of the last increment, where two cycles of loading were applied.

The Concrete01 material in OpenSees was used to simulate the confined and unconfined concrete in each wall. The maximum compression strength of confined concrete f'_{cc} was calculated based on the procedure outlined in ACI 550.7-19,[12] using the special boundary confinement reinforcement at the wall base and the measured compression strength of unconfined concrete f'_c. The connection tie reinforcement designed for the energy-dissipation bars was not considered in the confined concrete compression strength calculation. The confined concrete regions were assumed to be the areas enclosed by the centerlines of the special boundary confinement hoops at the ends of the wall (shaded in gray in Fig. 9). The ultimate strains of the unconfined concrete ε_{cu} and confined concrete ε_{ccu} were determined using the regularization method described in Pozo et al.[13] to reduce the mesh sensitivity of the analysis results (that is, sensitivity of the results to the number of numerical integration points) in the postpeak range of the wall lateral load–versus–drift behavior. The residual concrete compression strength was taken as 20% of the maximum compression strength for confined concrete and zero for unconfined concrete.

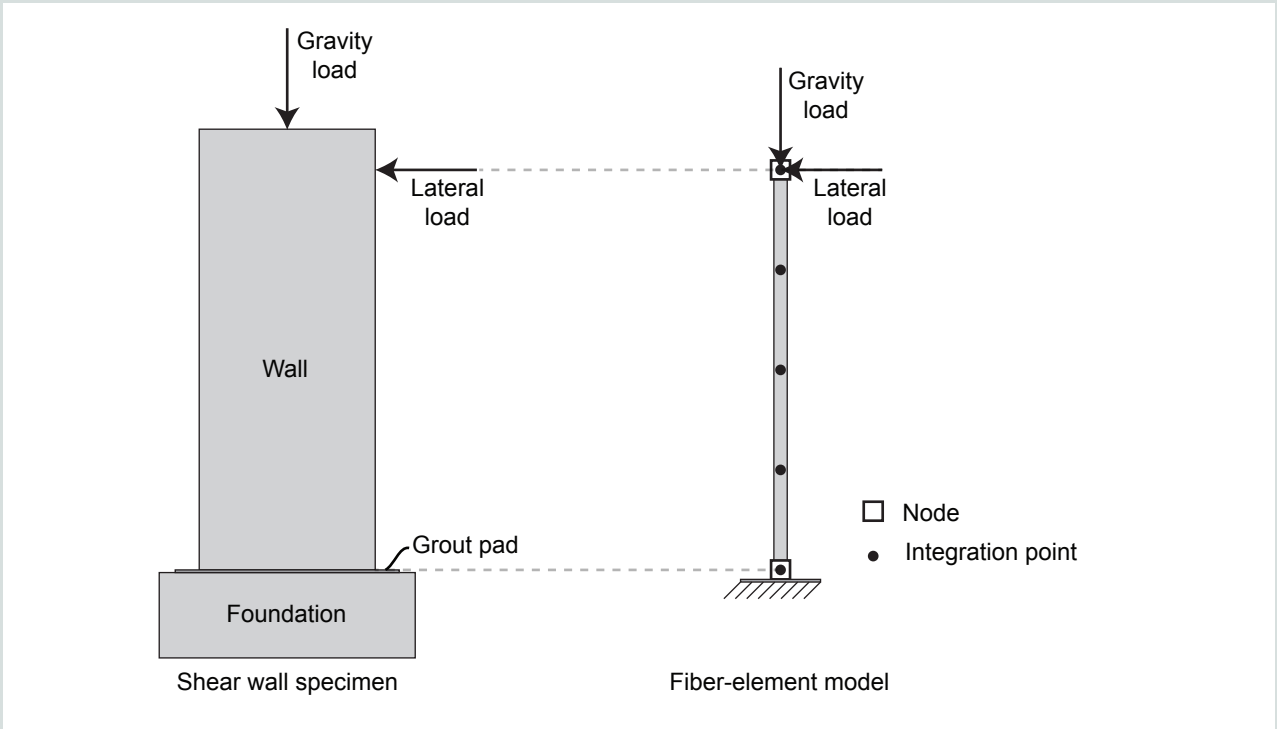

Figure 8. Fiber-element model elevation for test specimens.

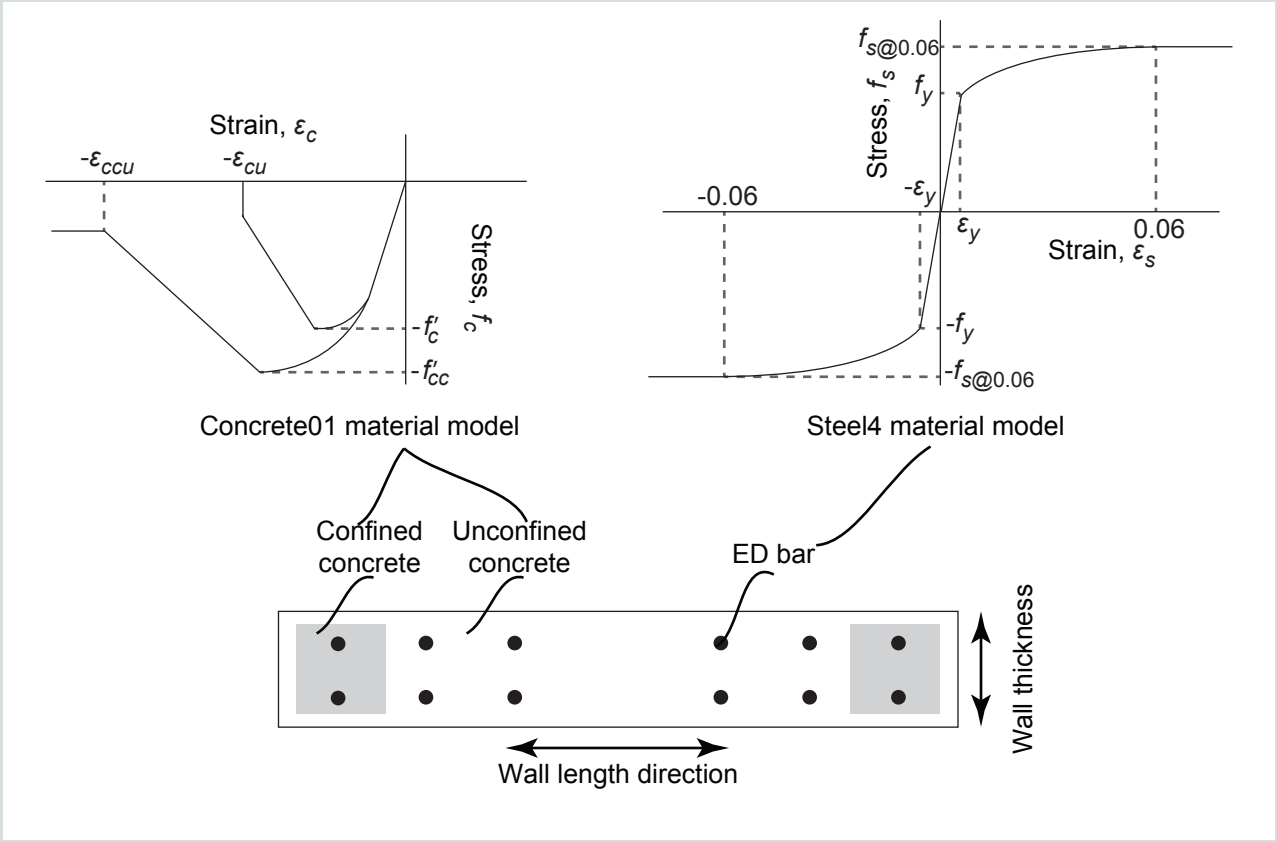

Figure 9. Concrete and steel fiber material models. Note: ED = energy-dissipation; f_c = stress of concrete; f'_c = compression strength of unconfined concrete; f'_{cc} = compression strength of confined concrete; f_s = stress of reinforcing bar; $f_{s@0.06}$ = stress from nonlinear monotonic stress-strain relationship of energy-dissipation bar at 0.06 in./in. strain; f_y = yield strength of reinforcing bar; ε_c = strain of concrete; ε_{ccu} = ultimate strain of confined concrete; ε_{cu} = ultimate strain of unconfined concrete; ε_s = strain of reinforcing bar; ε_y = yield strain of reinforcing bar.

The energy-dissipation bars were simulated using the Steel4 material model in OpenSees based on the measured nonlinear monotonic stress-strain relationship of the steel. The maximum strength of the reinforcing steel was limited to the stress corresponding to 0.06 in./in. (0.06 mm/mm) strain $f_{s@0.06}$ from the measured monotonic stress-strain relationship (Fig. 9). The application of this stress limit was informed by the maximum energy-dissipation bar stresses reported in Aragon et al.[2–4] for the validation of the short-grouted connections under uniaxial cyclic loading and considers reduction of bar strains (and therefore stresses) due to the intentional and any additional unbonding of the bars under cyclic loading, compared with stresses determined from bar strains calculated using section strain compatibility (that is, strains calculated assuming perfect bond with concrete). The tie reinforcement for the energy-dissipation bar connections was not modeled in the analyses. Instead, the energy-dissipation bars crossing the base joint were modeled as being fully developed inside the wall (perfect bond assumption) with no unbonding of the bars at the wall base. Fracture or pullout of the energy-dissipation bars was not modeled.

Figure 10 shows the measured and simulated reversed-cyclic base moment versus lateral drift behaviors for the six test specimens. In addition, the estimated trends for the ratio of compression length to wall length from the numerical models are compared with the measured trends in **Fig. 11**, where the compression length was calculated as the length from the extreme compression edge to the neutral axis location at the bottom of the wall (that is, the neutral axis length at the wall base). The numerical analysis results generally matched the measured base moment-drift behaviors of the specimens. The models estimated the ultimate failure of each wall to occur due to concrete crushing at the base, represented by postpeak reductions in base moment in Fig. 10. This concrete crushing failure was reflected as increases in the simulated compression length (Fig. 11) due to loss of compression stress (softening behavior of concrete in compression) during the large applied displacement cycles. The concrete crushing was more evident in the analyses of specimens 1, 2, and 3, which was likely because of the large compression demands induced by the large amount of energy-dissipation steel used in these specimens. As discussed in Al-Khateeb et al.,[5] specimens 2 and 3 experienced concrete crushing during testing (consistent with the analysis results), followed by pullout failure of the energy-dissipation bars inside the grouted connections. This bar pullout was not modeled and therefore not captured in the numerical analyses. For specimen 1, concrete crushing was

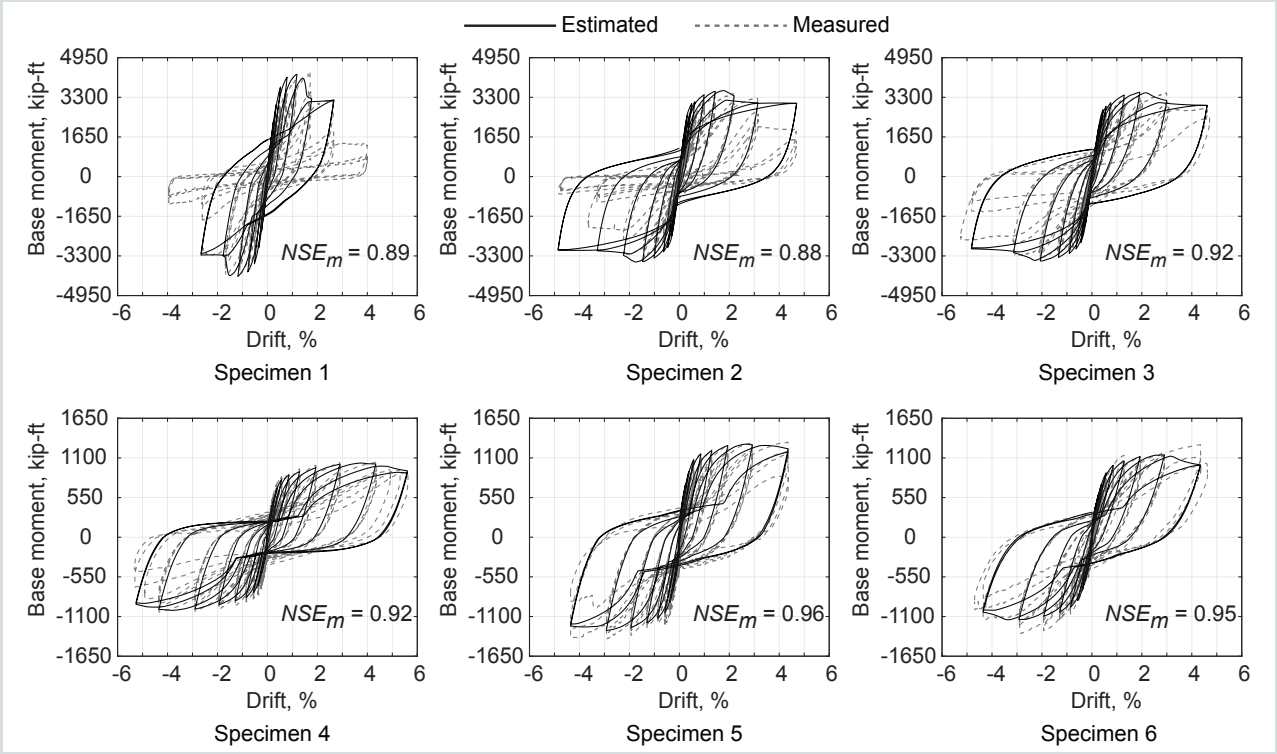

Figure 10. Estimated and measured base moment versus lateral drift behaviors. Note: NSE_m = modified Nash-Sutcliffe efficiency. 1 kip-ft = 1.356 kN-m.

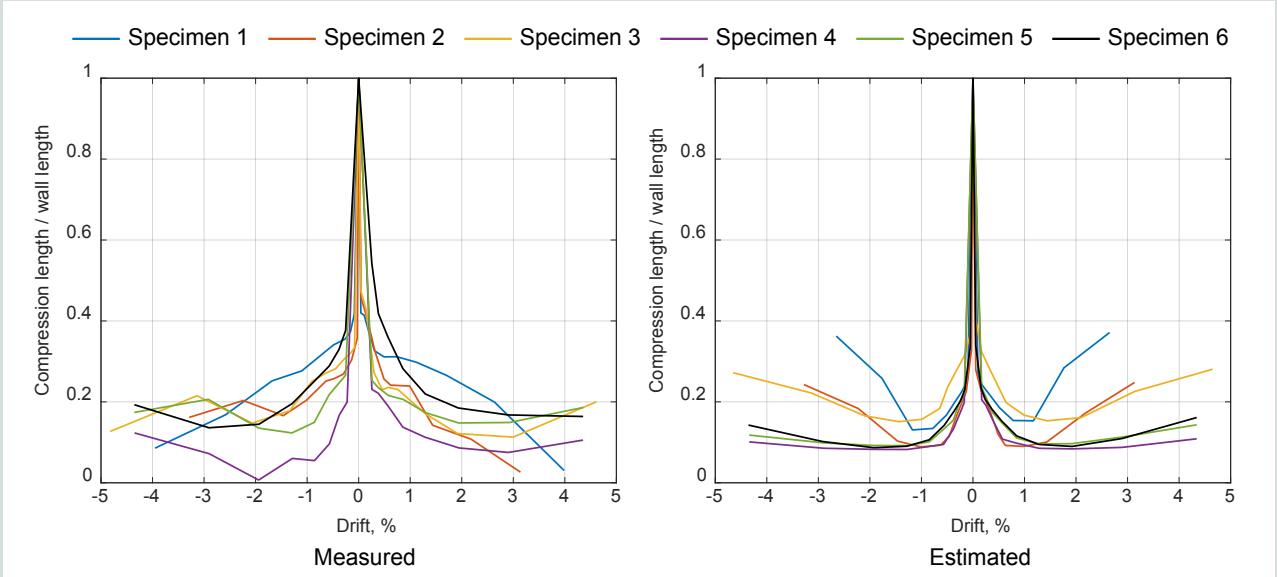

Figure 11. Estimated and measured compression (neutral axis) length-to-wall length ratio.

not observed during testing (as evident from the continuous decrease in the measured compression length in Fig. 11); this specimen failed because of a sudden breakout of the connection group in tension.[5] Specimen 1 included steel angles and compression-only vertical reinforcing bars at the wall toes, which prevented concrete crushing. These additional components were not considered in the numerical model, resulting in the discrepancy in the estimated failure mode.

For specimens 4, 5, and 6, the concrete crushing estimated by the numerical analyses was less significant, likely because of the smaller energy-dissipation bar areas used in these walls.

The axial load ratios for specimens 4, 5, and 6 were 0.013, 0.026, and 0.044, respectively, of $f'_c A_g$, where f'_c is the measured compression strength of unconfined concrete and A_g is the gross area of the wall cross section. These increasing axial load ratios and the associated increase in concrete crushing are reflected in larger growth of the estimated compression length during the large applied-displacement cycles when comparing specimens 4, 5, and 6 in Fig. 11. Because the numerical models did not include bar fracture, this failure mode observed in specimen 5 did not develop in the analyses.

The numerical analyses accurately estimated the measured maximum base moment strength of the test specimens, suggesting that limiting the maximum stress of the energy-dissipation bars to $f_{s@0.06}$ (Fig. 9) was able to indirectly account for the effects of intentional bar unbonding and any additional unbonding of the bars under cyclic loading. The model slightly underestimated the measured maximum strength for specimens 4, 5, and 6, which can be attributed to the better concrete confinement and improved force transfer around the connection ducts for these specimens as the final revision of the strut-and-tie model was implemented to design the tie reinforcement. Because the connection tie reinforcement was not considered in the confined concrete stress-strain model, the numerical analyses may have underestimated the concrete compression stresses in these walls. Quantitative comparisons for the maximum base moment strength of the test specimens are provided in the next section.

To evaluate the hysteretic wall behavior simulated by the numerical models, the modified Nash-Sutcliffe efficiency NSE_m metric was calculated up to the measured failure drift of each specimen (Fig. 10) following the procedure described in Pozo et al.[14] This metric incorporates both the traditional Nash-Sutcliffe efficiency[15] NSE and an energy error (error in the cumulative energy dissipated by the simulated base moment-drift curve with respect to the cumulative energy dissipated by the measured curve). The NSE_m values for specimens 1, 2, 3, 4, and 6 ranged from 0.88 to 0.95, indicating a satisfactory match between the numerical and experimental base moment-drift curves according to the evaluation criteria established by Pozo et al.[14] For specimen 5, the calculated NSE_m was 0.96, demonstrating a good match between the estimated and measured curves.

Overall, the comparisons of the nonlinear analysis results with the experimental measurements and observations presented in this paper show that conventional numerical modeling techniques for reinforced concrete structures can be used to analyze the nonlinear reversed-cyclic lateral load behavior of precast concrete shear walls with the proposed short-grouted energy-dissipation bar connections.

Nominal and probable axial-flexural strength

The nominal axial-flexural strength M_n of a precast concrete shear wall with short-grouted connections for the energy-dissipation bars (for example, at the wall-foundation joint interface) can be determined using conventional closed-form reinforced concrete section analysis procedures. In accordance with ACI 318-19[8] section 22.2.2.1, the extreme concrete compression strain ε_c is taken as 0.003. The concrete compression stress is assumed to be 0.85 times the unconfined concrete strength, uniformly distributed over an equivalent compression zone length of $\beta_1 c$, where β_1 is the factor for equivalent uniform concrete stress distribution per ACI 318-19 section 22.2.2.4.3, and c is the neutral axis length (that is, the length from the extreme concrete compression edge to the location of the neutral axis). The strain in the energy-dissipation bars at each layer is determined using section strain compatibility (**Fig. 12**). The corresponding stress in the energy-dissipation bars f_s is calculated as the strain in the steel ε_s times the modulus of elasticity E_s up to the steel yield strain ε_y. Beyond the yield point, the steel stress is limited to the yield strength f_y, as illustrated in the reinforcement model in Fig. 12.

The probable axial-flexural strength M_{pr} of the wall is calculated similarly to the nominal axial-flexural strength by assuming a uniformly distributed confined concrete compression stress of α times f'_{cc} over an equivalent uniform compression stress zone length of βc within the area covered by the centerlines of the confinement hoops. The procedure outlined in ACI 550.7-19[12] is used to determine the confined concrete compression strength f'_{cc}. The equivalent uniform confined concrete compression stress zone is based on ACI 550.7-19[12] and Sritharan et al.,[16] with α and β taken as 0.92 and 0.96, respectively (**Fig. 13**). ACI 550.7-19[12] and Sritharan et al.[16] recommend these values for simplicity of design as reasonable values for the range of unconfined concrete compression strengths f'_c between 4 and 8 ksi (27.6 and 55.2 MPa). A more detailed procedure for determining α and β is described in Sritharan et al.[16]

The extreme concrete compression strain is taken as the maximum usable strain of confined concrete ε_{cmax}, which is determined using the procedure in ACI 550.7-19.[12] The energy-dissipation bar strains are then determined based on section strain compatibility, and the corresponding stresses f_s are determined from the nonlinear monotonic stress-strain relationship of the bars. As described in the previous section on nonlinear numerical modeling, and, as the reinforcement model of Fig. 13 shows, the energy-dissipation bar stresses are limited to the stress corresponding to a strain of 0.06 in./in. (0.06 mm/mm) $f_{s@0.06}$.

Figure 14 compares the nominal and probable axial-flexural (base moment) strengths, determined using the aforementioned procedures, with the measured base moment–drift behavior of each wall test specimen. **Table 1** presents the maximum (peak) measured axial-flexural (base moment) strength M_{max} in the positive and negative directions of loading, the ratio of M_{max} to the probable axial-flexural strength M_{pr} calculated for the tested specimens, the ratio of M_{max} to the maximum base moment strength estimated by the OpenSees numerical model M_{mm} in each direction of loading

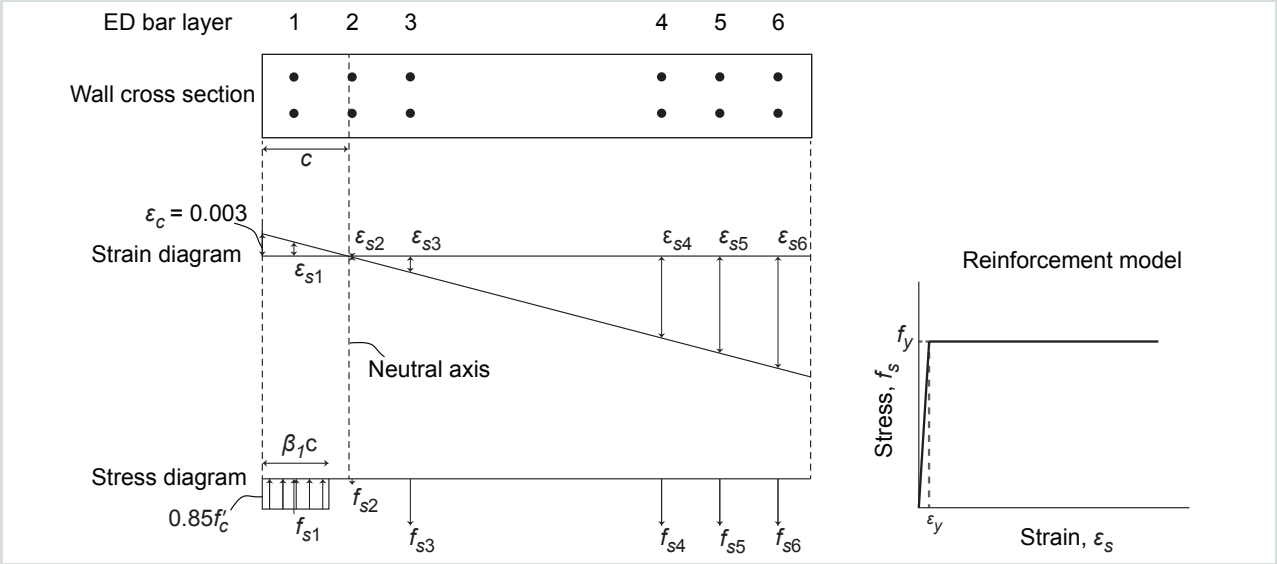

Figure 12. Wall section strain and stress distributions for nominal axial-flexural strength calculation. Note: c = neutral axis length (that is, length from extreme concrete compression edge to location of neutral axis); ED = energy-dissipation; f'_c = compression strength of unconfined concrete; f_s = stress of reinforcing bar; f_{s1} = stress of reinforcing bar at layer 1; f_{s2} = stress of reinforcing bar at layer 2; f_{s3} = stress of reinforcing bar at layer 3; f_{s4} = stress of reinforcing bar at layer 4; f_{s5} = stress of reinforcing bar at layer 5; f_{s6} = stress of reinforcing bar at layer 6; f_y = yield strength of reinforcing bar; β_1 = factor relating length of equivalent uniform unconfined concrete compression stress zone to neutral axis length; ε_c = strain of concrete; ε_s = strain of reinforcing bar; ε_{s1} = strain of reinforcing bar at layer 1; ε_{s2} = strain of reinforcing bar at layer 2; ε_{s3} = strain of reinforcing bar at layer 3; ε_{s4} = strain of reinforcing bar at layer 4; ε_{s5} = strain of reinforcing bar at layer 5; ε_{s6} = strain of reinforcing bar at layer 6; ε_y = yield strain of reinforcing bar.

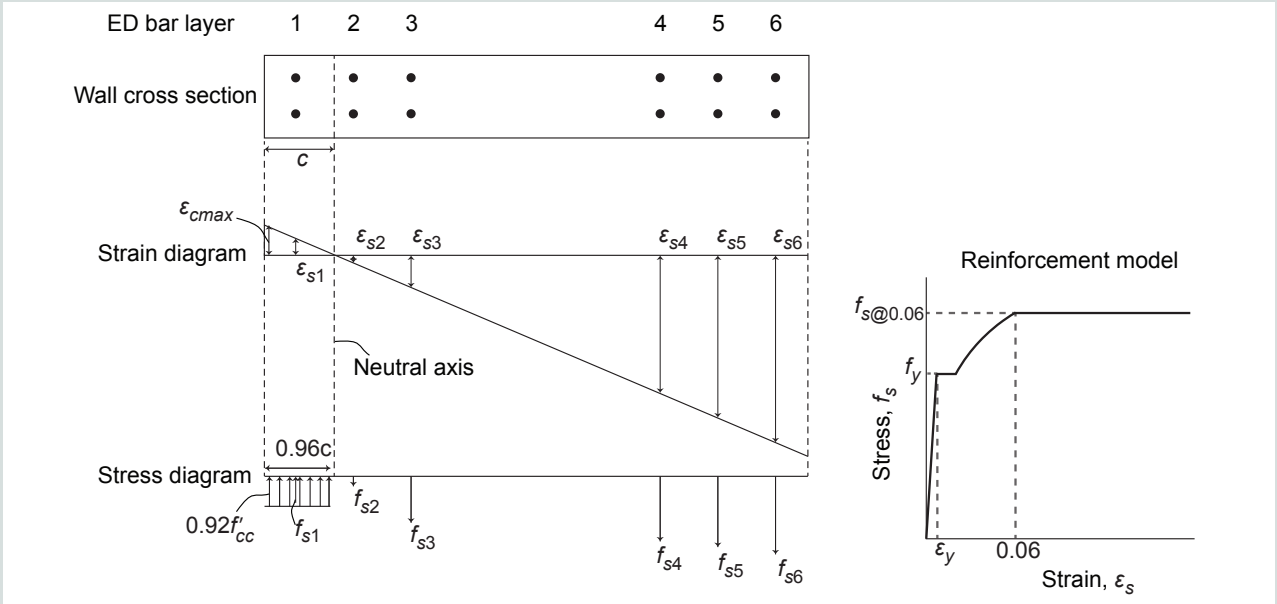

Figure 13. Wall section strain and stress distributions for probable axial-flexural strength calculation. Note: c = neutral axis length (that is, length from extreme concrete compression edge to location of neutral axis); ED = energy-dissipation; f'_{cc} = compression strength of confined concrete; f_s = stress of reinforcing bar; f_{s1} = stress of reinforcing bar at layer 1; f_{s2} = stress of reinforcing bar at layer 2; f_{s3} = stress of reinforcing bar at layer 3; f_{s4} = stress of reinforcing bar at layer 4; f_{s5} = stress of reinforcing bar at layer 5; f_{s6} = stress of reinforcing bar at layer 6; $f_{s@0.06}$ = stress from nonlinear monotonic stress-strain relationship of reinforcing bar at 0.06 in./in. strain; f_y = yield strength of reinforcing bar; ε_{cmax} = maximum usable strain of confined concrete; ε_s = strain of reinforcing bar; ε_{s1} = strain of reinforcing bar at layer 1; ε_{s2} = strain of reinforcing bar at layer 2; ε_{s3} = strain of reinforcing bar at layer 3; ε_{s4} = strain of reinforcing bar at layer 4; ε_{s5} = strain of reinforcing bar at layer 5; ε_{s6} = strain of reinforcing bar at layer 6; ε_y = yield strain of reinforcing bar. 1 in. = 25.4 mm.

(presented in the previous section), and the ratio of M_{max} to the calculated nominal axial-flexural strength M_n.

The M_{max}/M_{pr} ratios for all six specimens ranged from 0.82 to 1.09 (average of 0.96). The M_{max}/M_{pr} ratios for specimens 3, 4, 5, and 6 (which passed the applicable validation requirements of ACI 550.6-19[7]) were between 0.90 and 1.09 (average of 1.01), thus satisfying the 0.90 to 1.2 range specified by ACI 550.6-19 for each specimen. Focusing on specimens 3 through 6, the maximum measured base moment strength M_{max} to the maximum strength estimated by the OpenSees model M_{mm} ratio ranged between 0.97 and 1.17 (average of 1.05), and the ratio between M_{max} and M_n ranged between 1.11 and 1.37 (average of 1.23). These ratios confirm good correlation of the design calculations and numerical model results with the measured maximum strength,

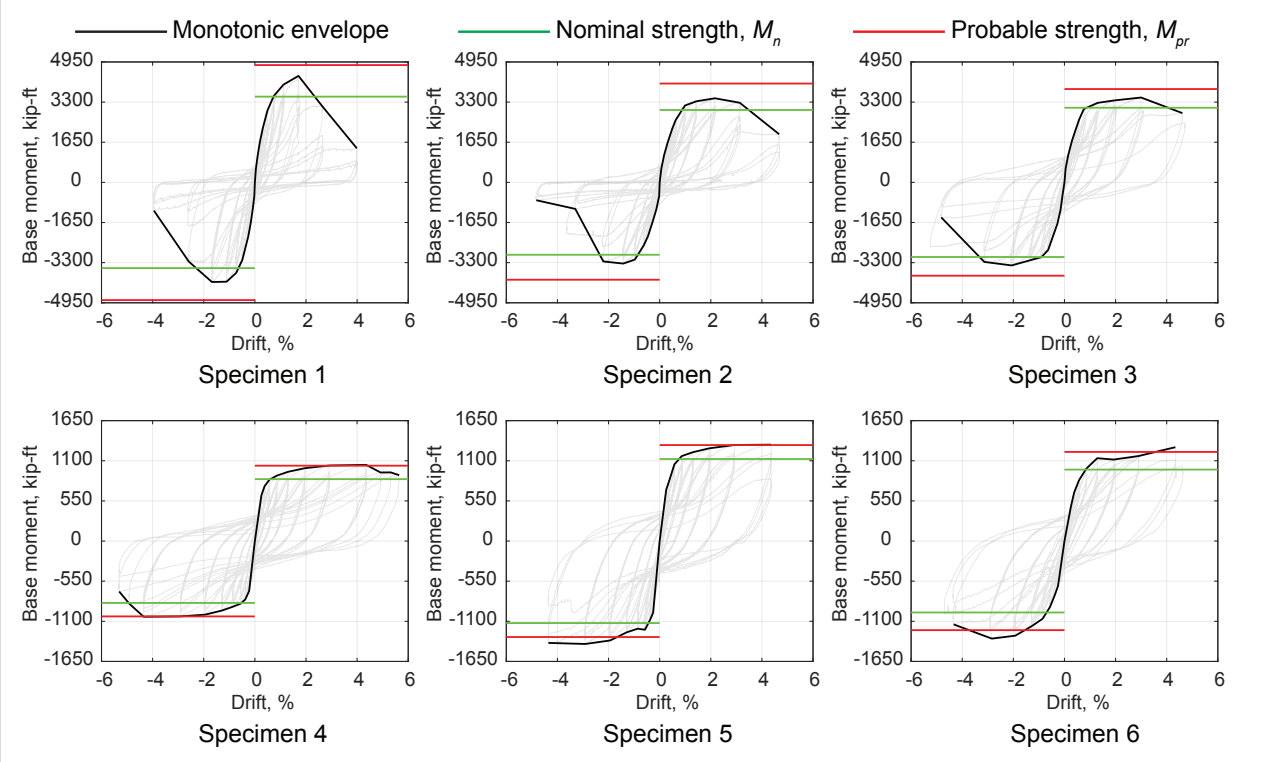

Figure 14. Nominal and probable axial-flexural (base moment) strengths of test specimens. Note: M_n = nominal axial-flexural (base moment) strength; M_{pr} = probable axial-flexural (base moment) strength. 1 kip-ft = 1.356 kN-m.

Table 1. Nominal and probable axial-flexural (base moment) strengths of test specimens

Specimen	M_{max}, kip-ft		$\frac{M_{max}}{M_{pr}}$		$\frac{M_{max}}{M_{mm}}$		$\frac{M_{max}}{M_n}$	
	+	-	+	-	+	-	+	-
1	4334	4092	0.89	0.84	1.03	0.98	1.24	1.16
2	3454	3333	0.85	0.82	0.96	0.94	1.16	1.12
3	3487	3410	0.92	0.90	0.99	0.97	1.14	1.11
4	1043	1038	1.01	1.01	1.01	1.02	1.23	1.22
5	1321	1410	1.01	1.08	1.02	1.09	1.18	1.25
6	1285	1336	1.05	1.09	1.13	1.17	1.31	1.37

Note: M_{max} = measured maximum (peak) axial-flexural (base moment) strength; M_{mm} = maximum (peak) axial-flexural (base moment) strength estimated by nonlinear numerical model; M_n = nominal axial-flexural (base moment) strength; M_{pr} = probable axial-flexural (base moment) strength.
1 kip-ft = 1.356 kN-m.

and reasonable overstrength of the test specimens compared with the calculated nominal axial-flexural strength. More detailed discussion of the calculated M_{pr} values for all six specimens follows.

Specimen 1 had M_{max}/M_{pr} values of 0.89 and 0.84 in the positive and negative directions of loading, respectively, indicating that the calculated probable axial-flexural strength overestimated the measured maximum strength. This overestimation, which exceeded the ACI 550.6-19 limit, was likely due to overestimation of the energy-dissipation bar strains (and thus the bar stresses). Specifically, because specimen 1 failed prematurely due to breakout of the connection group at each end of the wall,[5] it is likely that the energy-dissipation bars had smaller strains than the calculated strains when the wall reached M_{max}.

The calculated M_{pr} overestimated the measured maximum strength for specimen 2 as well, with M_{max}/M_{pr} ratios of 0.85 and 0.82 in the positive and negative loading directions, respectively, thus exceeding the ACI 550.6-19 limit in both directions. As discussed in Al-Khateeb et al.,[5] specimen 2 was not well confined at the bottom of the wall, contributing to its failure. However, the probable axial-flexural strength calculation assumed the wall to be well confined, leading to an overestimation of the concrete compression stresses and overestimation of the maximum base moment strength.

For specimen 3, the M_{max}/M_{pr} ratios were 0.92 and 0.90 in the positive and negative loading directions, respectively, also indicating overestimations of the wall maximum base moment strength, but within the ACI 550.6-19 limit. Similar to specimen 2, specimen 3 failed due to crushing of the concrete around the connections, followed by pullout of the energy-dissipation bars. However, as discussed in Al-Khateeb et al.,[5] the detailing modifications implemented in specimen 3 improved the confinement of concrete and transfer of forces around the connection ducts. This resulted in a better estimation of the maximum base moment strength for specimen 3 compared with specimen 2.

Specimens 4, 5, and 6 had M_{max}/M_{pr} ratios between 1.01 and 1.09, indicating small underestimations of the measured maximum base moment strength of the wall. This can be attributed to the improved design and detailing of tie reinforcement around the connections in these specimens, because the strut-and-tie model was revised after testing specimen 3.[6] As another potential contributor, the base moment-to-shear ratio of specimens 4 through 6 was greater than that of specimens 1 through 3 (ratio of 3 compared with 2 times the wall length, respectively). This difference resulted in greater contribution of flexural deformations to the lateral load behavior of specimens 4 through 6 (as compared with specimens 2 and 3),[5,6] leading to better alignment with the axial-flexural analysis procedures. The maximum base moment strength M_{mm} estimated by the nonlinear numerical model for specimens 4, 5, and 6 (M_{max}/M_{mm} ratios between 1.01 and 1.17) were consistent with the M_{pr} results from the closed-form probable axial-flexural strength calculation procedure. This indicates that for walls with short-grouted energy-dissipation bar connections designed and detailed as described in this paper, both the proposed closed-form probable strength calculation procedure and the nonlinear numerical model results provide reasonable estimations of the actual maximum base moment strength.

It should be noted that the M_{max}/M_{pr} ratios presented in Al-Khateeb et al.[5] for specimens 1, 2, and 3 differ from the corresponding values in Table 1 because of three differences in the calculation of M_{pr}. Specifically, in Al-Khateeb et al.,[5]

- The concrete stresses in the compression zone were estimated using the Hognestad et al.[17] unconfined concrete stress-strain relationship (rather than the uniform confined concrete stress of $0.92f'_{cc}$ described herein).
- The energy-dissipation bar strains were estimated using strain compatibility with a maximum Hognestad et al.[17] unconfined concrete compression strain of 0.0038 (rather than the maximum usable confined concrete strain ε_{cmax}).
- The energy-dissipation bar stresses were obtained from the nonlinear monotonic stress-strain relationship of the steel without any limit (rather than limiting the maximum energy-dissipation bar stresses to $f_{s@0.06}$).

The revised procedure presented in this paper is ultimately recommended based on the test results from all six wall specimens.

Conclusion

This paper presents design, detailing, and analysis recommendations for nonproprietary, short-grouted, corrugated steel straight duct connections for energy-dissipation bars crossing horizontal joints in precast concrete shear walls. Design examples are presented in "Design, Detailing, and Analysis of Short-Grouted Ductile Reinforcing Bar Connections for Special Precast Concrete Shear Walls, Part 2: Short-Grouted Ductile Reinforcing Bar Connection Design Examples" on pages 78 through 104[9] The connection design approach is based on a strut-and-tie model to determine the connection length as well as the amount and detailing of tie reinforcement around the ducts. Closed-form procedures for estimating the nominal and probable (maximum) axial-flexural strengths of walls incorporating these connections are described. In addition, numerical analysis results using conventional fiber-element models are compared with the wall test results. The following conclusions are drawn from the study:

- The minimum required vertical tie reinforcement area A_{vt}, transverse tie reinforcement area A_{tt}, longitudinal tie reinforcement area A_{lt}, and connection length l_{ED} can be calculated using Eq. (2), (3), (12), (17), and (18).

- U bars should be used to serve as both vertical and transverse tie reinforcement around the connection ducts. Thus, Eq. (3) for the transverse tie reinforcement area A_{tt} is automatically satisfied and does not need to be checked.

- The energy-dissipation bars should be intentionally unbonded within the horizontal joint grout pad and over a length of $3d_{ED}$ inside the connection ducts (that is, within the connection length l_{ED}) immediately adjacent to the horizontal joint grout pad.

- Placement of the longitudinal tie bars is a key factor in the effectiveness of the connection reinforcement. To optimize the connection design, the longitudinal tie reinforcement should engage the U bars and the centroid of the longitudinal tie bars should be located as close as possible to the transverse (horizontal) legs of the U bars (reducing the $S_{c,UL}$ distance).

- Although it is permissible to design connections where the longitudinal tie reinforcement area is limited to the maximum effective area of $1.5A_{ED}$, this design will result in longer connections by shifting the strut-and-tie model work point farther away from the centroid of the longitudinal tie reinforcement.

- The minimum 28-day compression strength of the energy-dissipation bar connection grout and the horizontal joint pad grout should be specified as 9.00 ksi (62.1 MPa). The connection grout should be in pumpable consistency according to the grout manufacturer's recommendations. Both the connection grout and the horizontal joint pad grout should be placed without any voids, air pockets, or other defects. To limit deterioration of the horizontal joint grout pad during the lateral displacements of the wall subjected to a large earthquake, polypropylene fibers (dosage per the fiber manufacturer) should be added to the grout at horizontal joints where nonlinear behavior of the wall is expected. Dry packing of this grout is not recommended because it is difficult to ensure that the grout is adequately compacted without voids over the entire joint volume with this method.

- A minimum cumulative corrugation depth of 1.25 in./ft (104 mm/m) should be specified for the connection ducts to ensure sufficient mechanical interlock of the ducts with the connection grout and the wall concrete.

- The reversed-cyclic hysteretic lateral load behavior of precast concrete shear walls with short-grouted energy-dissipation bar connections can be simulated using conventional numerical modeling approaches commonly adopted for the analysis of reinforced concrete shear walls. The measured maximum lateral strength–to–numerical model strength ratio M_{max}/M_{mm} for all specimens ranged from 0.94 to 1.17, with an average of 1.03.

- The nominal axial-flexural strength of precast concrete shear walls with short-grouted energy-dissipation bar connections can be determined using conventional closed-form reinforced concrete section analysis procedures with the compression strength of unconfined concrete and the yield strength of the energy-dissipation bars.

- The probable (maximum) axial-flexural strength of precast concrete shear walls with short-grouted energy-dissipation bar connections can similarly be determined using conventional closed-form reinforced concrete section analysis procedures. This calculation uses the compression strength of confined concrete and the nonlinear stress-strain relationship of the energy-dissipation bars, with the energy-dissipation bar stresses limited to the stress corresponding to 0.06 in./in. (0.06 mm/mm) strain $f_{s@0.06}$. For specimens 3, 4, 5, and 6, which passed the applicable validation requirements of ACI 550.6-19, the measured maximum lateral strength–to–calculated probable strength ratio M_{max}/M_{pr} ranged from 0.90 to 1.09, within the acceptable range of 0.90 through 1.20 specified by ACI 550.6-19.

Acknowledgments

This research was conducted with funding from the Charles Pankow Foundation, PCI, Clark Pacific, and Metromont Corp., and the test specimens were donated by Clark Pacific and Metromont Corp. This support is gratefully acknowledged. The authors thank the PCI Research and Development Council and the PCI Central Region, as well as members of the Industry Advisory Committee, including Suzanne Aultman of Metromont Corp.; Keith Bauer of Buehler Engineering; Kal Benuska of John A. Martin and Associates; Jared Brewe of S.K. Ghosh Associates LLC (formerly of PCI); Harry Gleich of Gleich Engineering and Associates LLC (formerly of Metromont Corp.); Les Kempers of GPRM Prestress; Kevin Kirkley of Tindall Corp.; Walter Korkosz of Consulting Engineers Group; Donald Meinheit of Wiss, Janney, Elstner Associates; Andrew Osborn of Wiss, Janney, Elstner Associates; and Wael Zatar of Marshall University. The authors also thank StresCore Inc. for assisting in handling the test specimens. Any opinions, findings, conclusions, and recommendations expressed in the paper are those of the authors and do not necessarily reflect the views of the individuals and organizations acknowledged.

References

1. Smith, B. J., Y. C. Kurama, and M. J. McGinnis. 2013. "Behavior of Precast Concrete Shear Walls for Seismic Regions: Comparison of Hybrid and Emulative Specimens." *Journal of Structural Engineering* 139 (11): 1917–1927.

2. Aragon, T. A., Y. C. Kurama, and D. F. Meinheit. 2017. "A Type III Grouted Seismic Connector for Precast Concrete Structures." *PCI Journal* 62 (5): 75–88.

3. Aragon, T. A., Y. C. Kurama, and D. F. Meinheit. 2019. "Effects of Grout and Energy Dissipating Bar Properties on a Type III Grouted Seismic Connection for Precast Structures." *PCI Journal* 64 (1): 31–48.

4. Aragon, T. A., Y. C. Kurama, and D. F. Meinheit. 2020. "Behavior of Ductile Short-Grouted Seismic Reinforcing Bar-to-Foundation Connections Under Adverse Construction Conditions." *PCI Journal* 65 (4): 33–50.

5. Al-Khateeb, B., C. Garcia, M. P. Manning, J. Mohle, and Y. C. Kurama. 2025. "Seismic Precast Concrete Shear Walls with Short-Grouted Ductile Reinforcing Bar Connections." *PCI Journal* 70 (1): 58–83.

6. Al-Khateeb, B., J. Mohle, and Y. C. Kurama. 2025. "Performance of Short-Grouted Ductile Reinforcing Bar Connections under Varying Design Parameters." *PCI Journal* 70 (6): 17–38.

7. ACI Innovation Task Group 5. 2019. *Acceptance Criteria for Special Unbonded Post-Tensioned Precast Structural Walls Based on Validation Testing and Commentary*. ACI 550.6. Farmington Hills, MI: ACI.

8. ACI (American Concrete Institute) Committee 318. 2019. *Building Code Requirements for Structural Concrete (ACI 318-19) and Commentary (ACI 318R-19)*. Farmington Hills, MI: ACI.

9. Al-Khateeb, B., J. Mohle, and Y. C. Kurama. 2026. "Design, Detailing, and Analysis of Short-Grouted Ductile Reinforcing Bar Connections for Special Precast Concrete Shear Walls, Part 2: Short-Grouted Ductile Reinforcing Bar Connection Design Examples." *PCI Journal* 71 (3): 78–104. https://doi.org/10.15554/pcij71.3-03.

10. ASTM Subcommittee A01.05. 2016. *Standard Specification for Deformed and Plain Low-Alloy Steel Bars for Concrete Reinforcement*. ASTM A706/A706M. West Conshohocken, PA: ASTM International.

11. Barbachyn, S. M., Y. C. Kurama, M. J. McGinnis, and R. Sause. 2016. "Coupled Shear Wall with Fully Post-tensioned Beams and Unbonded Rebar at Toes." *ACI Structural Journal* 113 (6): 1381–1392.

12. ACI Innovation Task Group 5. 2019. *Requirements for Design of a Special Unbonded Post-Tensioned Precast Shear Wall Satisfying ACI 550.6 and Commentary*. ACI 550.7. Farmington Hills, MI: ACI.

13. Pozo, J. D., M. A. Hube, and Y. C. Kurama. 2021. "Effect of Material Regularization in Plastic Hinge Integration Analysis of Slender Planar RC Walls." *Engineering Structures* 239 (15): 112302.

14. Pozo, J. D., M. A. Hube, and Y. C. Kurama. 2020. "Quantitative Assessment of Nonlinear Macro-Models for Global Behavior and Design of Planar RC Walls." *Engineering Structures*, no. 224, 111190.

15. Nash, J. E., and J. V. Sutcliffe. 1970. "River Flow Forecasting through Conceptual Models Part I—A Discussion of Principles." *Journal of Hydrology* 10 (3): 282–290.

16. Sritharan, S., Sriram Aaleti, and Derek J. Thomas. 2007. "Seismic Analysis and Design of Precast Concrete Jointed Wall Systems." Iowa State University ISU-ERI-Ames report ERI-07404. Ames, IA: Iowa State University.

17. Hognestad, E. 1951. "A Study of Combined Bending and Axial Load in Reinforced Concrete Members." University of Illinois bulletin no. 399. Urbana, IL: University of Illinois at Urbana-Champaign.

Notation

A_{ED} = total area of energy-dissipation bar or bars in one layer across thickness of wall cross section

A_g = gross area of wall cross section

A_{lt} = total required area of longitudinal tie reinforcement to transfer tension force in A_{ED}

A_{tt} = total required area of transverse tie reinforcement to transfer tension force in A_{ED}

A_{vt} = total required area of vertical tie reinforcement to transfer tension force in A_{ED}

c = neutral axis length (length from extreme concrete compression edge to location of neutral axis)

C = clear vertical cover to U bars

d_{duct} = inner diameter of connection duct

d_{ED} = diameter of energy-dissipation bar

d_U = diameter of U bar

D = distance between center of energy-dissipation bar and center of vertical leg of U bar

E_s = modulus of elasticity of reinforcing bar

f_c = stress of concrete

f'_c = compression strength of unconfined concrete

f'_{cc} = compression strength of confined concrete

f_s = stress of reinforcing bar

f_{s1} = stress of reinforcing bar at layer 1

f_{s2} = stress of reinforcing bar at layer 2

f_{s3} = stress of reinforcing bar at layer 3

f_{s4} = stress of reinforcing bar at layer 4

f_{s5} = stress of reinforcing bar at layer 5

f_{s6} = stress of reinforcing bar at layer 6

$f_{s@0.06}$ = stress from nonlinear monotonic stress-strain relationship of energy-dissipation bar at 0.06 in./in. strain

$f_{u,vt}$ = ultimate (peak) strength of vertical tie bar

f_y = yield strength of reinforcing bar

$f_{y,ED}$ = yield strength of energy-dissipation bar

$f_{y,lt}$ = yield strength of longitudinal tie bar

$f_{y,vt}$ = yield strength of vertical tie bar

h_{wp} = height of strut-and-tie model work point measured from center of transverse tie (horizontal leg of U bar) projected onto energy-dissipation bar

K = longitudinal tie reinforcement area multiplier

l_b' = prescribed minimum grouted bond length extension (beyond strut-and-tie model work point) of 9 times bar diameter for no. 7, 8, and 9 (22M, 25M, and 29M) energy-dissipating bars and 12 times bar diameter for no. 10 and 11 (32M and 36M) bars

l_d = development length of reinforcing bar

l_{ED} = length of energy-dissipation bar inside connection duct

l_U = required length of vertical legs of U bars

M_b = wall base moment

M_{max} = maximum (peak) measured axial-flexural (base moment) strength

M_{mm} = maximum (peak) axial-flexural (base moment) strength estimated by nonlinear numerical model

M_n = nominal axial-flexural (base moment) strength

M_{pr} = probable axial-flexural (base moment) strength

NSE = Nash-Sutcliffe efficiency

NSE_m = modified Nash-Sutcliffe efficiency

R = ratio between ultimate (peak) strength of vertical tie reinforcing steel and yield strength of longitudinal tie reinforcing steel

$S_{c,UL}$ = vertical distance between center of transverse tie bar (horizontal leg of U bar) and centroid of longitudinal tie reinforcement

V_b = wall base shear force

X = horizontal distance between center of energy-dissipation reinforcing bar and center of vertical tie bar (vertical leg of U bar) in wall length direction

X_1 = horizontal distance between center of energy-dissipation reinforcing bar and center of vertical tie bar (vertical leg of U bar) in wall length direction, sample 1

X_2 = horizontal distance between center of energy-dissipation reinforcing bar and center of vertical tie bar (vertical leg of U bar) in wall length direction, sample 2

Y = horizontal distance between center of energy-dissipation reinforcing bar and center of vertical tie bar (vertical leg of U bar) in wall thickness direction

Y_1 = horizontal distance between center of energy-dissipation reinforcing bar and center of vertical tie bar (vertical leg of U bar) in wall thickness direction, sample 1

Y_2 = horizontal distance between center of energy-dissipation reinforcing bar and center of vertical tie bar (vertical leg of U bar) in wall thickness direction, sample 2

α = factor relating stress of equivalent uniform confined concrete compression stress zone at M_{pr} to compression strength of confined concrete

β = factor relating length of equivalent uniform confined concrete compression stress zone to neutral axis length at M_{pr}

β_{lt} = horizontal plane angle of strut-and-tie model (complementary to β_{tt})

β_{lt1} = horizontal plane angle of strut-and-tie model (complementary to β_{tt}), sample 1

β_{lt2} = horizontal plane angle of strut-and-tie model (complementary to β_{tt}), sample 2

β_{tt} = horizontal plane angle of strut-and-tie model (complementary to β_{lt})

β_1 = factor relating length of equivalent uniform unconfined concrete compression stress zone to neutral axis length at M_n

ε_c = strain of concrete

ε_{ccu} = ultimate strain of confined concrete

ε_{cmax} = maximum usable strain of confined concrete

ε_{cu} = ultimate strain of unconfined concrete

ε_s = strain of reinforcing bar

ε_{s1} = strain of reinforcing bar at layer 1

ε_{s2} = strain of reinforcing bar at layer 2

ε_{s3} = strain of reinforcing bar at layer 3

ε_{s4} = strain of reinforcing bar at layer 4

ε_{s5} = strain of reinforcing bar at layer 5

ε_{s6} = strain of reinforcing bar at layer 6

ε_y = yield strain of reinforcing bar

θ = vertical plane angle of strut-and-tie model between work point and transverse tie node

θ' = vertical plane angle of strut-and-tie model between work point and longitudinal tie node

θ'_1 = vertical plane angle of strut-and-tie model between work point and longitudinal tie node, sample 1

θ'_2 = vertical plane angle of strut-and-tie model between work point and longitudinal tie node, sample 2

About the authors

Baha'a Al-Khateeb, PhD, is a structural project engineer at Frost Engineering and Consulting in Mishawaka, Ind. At the time this research was performed, he was a graduate student in the Department of Civil and Environmental Engineering and Earth Sciences at the University of Notre Dame in Notre Dame, Ind.

Jon Mohle, SE, is director of product innovation at Clark Pacific in Sacramento, Calif.

Yahya C. Kurama, PhD, PE, is a professor in the Department of Civil and Environmental Engineering and Earth Sciences at the University of Notre Dame.

Abstract

This paper presents design, detailing, and analysis recommendations for nonproprietary short-grouted ductile energy-dissipation bar connections in special seismic precast concrete shear walls. The performance of the connections was experimentally validated based on previous testing of six shear wall specimens in accordance with ACI 550.6-19. Vertical, transverse, and longitudinal tie reinforcing bars were designed for the connections to transfer the energy-dissipation bar forces into the precast concrete components. A strut-and-tie model was developed and validated to design the tie reinforcement and connection length of the energy-dissipation bars to meet the specified performance objectives. Simplified equations are presented in this paper for practicing engineers to design precast concrete components that use these connections without going into the details of the strut-and-tie model. Conventional closed-form section analysis procedures to predict the nominal and probable axial-flexural strengths of walls using short-grouted energy-dissipation bar connections are presented and validated against the measured behaviors of the tested specimens. In addition, results from nonlinear fiber-element analyses are compared with the experimental data to demonstrate that precast concrete walls with short-grouted connections can be simulated numerically using techniques commonly adopted for reinforced concrete shear walls. The connection design procedure is demonstrated on numerical examples of realistic wall cross sections covering a wide range of properties in an accompanying article.

Keywords

Energy-dissipation bar, mechanical grouted connection, nominal and probable axial-flexural strength, reinforcing bar connector, special shear wall, strut-and-tie design model, unbonding.

Review policy

This paper was reviewed in accordance with the Precast/Prestressed Concrete Institute's peer-review process. The Precast/Prestressed Concrete Institute is not responsible for statements made by authors of papers in *PCI Journal*. No payment is offered.

Publishing details

This paper appears in *PCI Journal* (ISSN 0887-9672) V. 71, No. 3, May–June 2026, and can be found at https://doi.org/10.15554/pcij71.3-02. *PCI Journal* is published bimonthly by the Precast/Prestressed Concrete Institute, 8770 W. Bryn Mawr Ave., Suite 1150, Chicago, IL 60631.

Copyright © 2026, Precast/Prestressed Concrete Institute.

Reader comments

Please address any reader comments to journal@pci.org or Precast/Prestressed Concrete Institute, c/o *PCI Journal*, 8770 W. Bryn Mawr Ave., Suite 1150, Chicago, IL 60631.